OKINAWA INSTITUTE OF SCIENCE AND TECHNOLOGY GRADUATE UNIVERSITY
沖縄科学技術大学院大学

Colorectal carcinoma: Ex vivo evaluation using q-space imaging; Correlation with histopathologic findings

Author	Ichiro Yamada, Keigo Hikishima, Norio Yoshino, Junichiro Sakamoto, Naoyuki Miyasaka, Shinichi Yamauchi, Hiroyuki Uetake, Masamichi Yasuno, Yukihisa Saida, Ukihide Tateishi, Daisuke Kobayashi, Yoshinobu Eishi
journal or publication title	Journal of Magnetic Resonance Imaging
volume	48
number	4
page range	1059-1068
year	2018-03-30
Publisher	John Wiley & Sons, Inc.
Rights	(C) 2018 International Society for Magnetic Resonance in Medicine This is the peer reviewed version of the following article: Yamada, I. , Hikishima, K. , Yoshino, N , Sakamoto, J. , Miyasaka, N , Yamauchi, S. , Uetake, H , Yasuno, M , Saida, Y. , Tateishi, U , Kobayashi, D. and Eishi, Y. (2018), Colorectal carcinoma: Ex vivo evaluation using q space imaging; Correlation with histopathologic findings. J. Magn. Reson. Imaging, 48: 1059-1068. doi:10.1002/jmri.26018, which has been published in final format https://doi.org/10.1002/jmri.26018. This article may be used for non-commercial purposes in accordance with Wiley Terms and Conditions for Use of Self-Archived Versions.
Author's flag	author
URL	http://id.nii.ac.jp/1394/00000674/

doi: info:doi/10.1002/jmri.26018

Colorectal Carcinoma: Ex Vivo Evaluation using q-Space Imaging; Correlation with Histopathologic Findings

Ichiro Yamada, MD,[1]* Keigo Hikishima, PhD,[2] Norio Yoshino, DDS,[3] Junichiro Sakamoto, DDS,[3] Naoyuki Miyasaka, MD,[4] Shinichi Yamauchi, MD,[5] Hiroyuki Uetake, MD,[5] Masamichi Yasuno, MD,[5] Yukihisa Saida, MD,[1] Ukihide Tateishi, MD,[1] Daisuke Kobayashi, MD,[6] and Yoshinobu Eishi, MD[6]

Footnotes: From the [1]Department of Diagnostic Radiology and Nuclear Medicine, Graduate School, Tokyo Medical and Dental University, Tokyo, Japan.
[2]Okinawa Institute of Science and Technology Graduate University, Okinawa, Japan.
[3]Department of Oral and Maxillofacial Radiology, Tokyo Medical and Dental University, Tokyo, Japan.
[4]Department of Comprehensive Reproductive Medicine, Tokyo Medical and Dental University, Tokyo, Japan.
[5]Department of Colorectal Surgery, Tokyo Medical and Dental University, Tokyo, Japan.
[6]Department of Pathology, Tokyo Medical and Dental University, Tokyo, Japan.

* Address reprint requests to: I.Y., Department of Diagnostic Radiology and Nuclear Medicine, Graduate School, Tokyo Medical and Dental University, 1-5-45 Yushima, Bunkyo-ku, Tokyo 113-8519, Japan. E-mail: yamada.crad@tmd.ac.jp

Address for correspondence:
Ichiro Yamada, MD,
Department of Diagnostic Radiology and Nuclear Medicine,
Graduate School, Tokyo Medical and Dental University,
1-5-45 Yushima, Bunkyo-ku, Tokyo 113-8519, Japan.
Telephone: 81-3-5803-5310. FAX: 81-3-5803-0147.
E-mail: yamada.crad@tmd.ac.jp

Running Title: q-Space Imaging of Colorectal Carcinoma

Colorectal Carcinoma: Ex Vivo Evaluation using q-Space Imaging; Correlation with Histopathologic Findings

2

Abstract

Background: Although the prognosis of colorectal carcinoma (CRC) patients depends on the histologic grade (HG) and lymph node metastasis (LNM), accurate preoperative assessment of these prognostic factors is often difficult.

Purpose: To assess the HG and extent of LNM by q-space imaging (QSI) for preoperative diagnosis of CRC.

Study Type: Prospective.

Specimen: A total of 20 colorectal tissue samples containing adenocarcinomas and resected lymph nodes (LNs).

Field Strength/Sequence: QSI was performed with a 3-T MRI system using a diffusion-weighted echo-planar imaging sequence: repetition time, 10000 ms; echo time, 216 or 210 ms; field of view, 113 × 73.45 mm; matrix, 120 × 78; section thickness, 4 mm; and 11 b values ranging from 0 to 9000 s/mm^2.

Assessment: The mean displacement (MDP; μm), zero-displacement probability (ZDP; arbitrary unit [a.u.]), kurtosis (K; a.u.), and apparent diffusion coefficient (ADC) were analyzed by two observers and compared with histopathologic findings.

Statistical Tests: The Spearman's rank correlation coefficient, Mann-Whitney U-test, and ROC curve analyses.

Results: For all 20 carcinomas, the MDP, ZDP, K, and ADC were 8.87 ± 0.37 μm, 82.0 ± 6.2 a.u., 74.3 ± 3.0 a.u., and 0.219 ± 0.040 x 10^{-3} mm^2/s, respectively. The MDP (r = −0.768; P < 0.001), ZDP (r = 0.768; P < 0.001), and K (r = 0.785; P < 0.001) were significantly correlated with the HG of CRC, but not the ADC (r = 0.088; P = 0.712). There were also significant differences in the MDP, ZDP, and K between metastatic and non-metastatic LNs (all, P < 0.001), but not the ADC (P = 0.082). In the HG of CRC and LNM, the area under the curve was significantly greater for MDP, ZDP, and K than for ADC.

Data Conclusion: QSI provides useful diagnostic information to assess the HG and extent of LNM in CRC.

Key Words: colon; rectum; colorectal carcinoma; q-space imaging; diffusion-weighted imaging; MR imaging

Introduction

Colorectal carcinoma (CRC) is a common and often lethal malignant neoplasm that is prognosticated based on the histologic grade (HG) and the presence and extent of lymph node metastasis (LNM). Careful evaluation of these factors before surgery has a decisive influence on the choice of therapy for CRC (1,2).

CRC staging before surgery is presently based on the findings of computed tomography (CT) and endoscopic ultrasound (EUS), even though it is not possible to accurately assess the HG and extent of LNM by imaging alone because CT has poor soft-tissue contrast and nonspecific size criteria (3,4), and EUS is limited by technical inadequacies to detect stenotic tumors, extraordinary operator reliance, interface echoes caused by artifacts, and an inadequate sonographic range (5-7). Although conventional magnetic resonance imaging (MRI) is an alternative to CT and EUS (8,9), this method is insufficient to assess the HG and extent of LNM in CRC (10-19).

Overall, current diagnostic procedures for the diagnosis of CRC are relatively limited. To overcome these limitations, Yamada et al. (20,21) recently reported that non-Gaussian q-space imaging (QSI) was suitable for ex vivo assessment of the HG and extent of LNM in esophageal and gastric carcinomas.

Hence, the aim of the present study was to evaluate the usefulness of QSI to prospectively assess the HG and extent of LNM of surgical adenocarcinoma tissue samples collected from the colon and rectum.

Materials and Methods

Study Population

A total of 20 surgical tissue samples of histologically confirmed adenocarcinoma surrounded by normal colorectal tissue and lymph nodes (LNs) resected from 20 consecutive patients (13 men and 7 women; mean age, 67 ± 9 years; age range, 51−82 years) who were treated at the Department of Colorectal Surgery were included for analysis. All tissue samples were included in a previous study of high-spatial-resolution MRI (22). After fixation in 10% formalin, the tissue samples were imaged. In vivo examinations of the colon and rectum were not performed in this study. The study protocol was approved by the local institutional review board and all study participants provided written informed consent.

Imaging Technique

QSI was performed with a 3-T MRI system (Magnetom Spectra; Siemens, Erlangen, Germany) fitted with actively shielded gradients with a maximum power of 33 mT/m. All measurements were accumulated using a 4-channel phased-array surface coil (Figure 1a). After immersion of the resected colorectal specimen in water and setting the container on a surface coil, the QSI orientation was set longitudinally along the longest axis of the specimen. The resected LNs were immersed in small flasks of water, which were then immersed in the container of water on the surface coil (Figure 1b).

QSI data sets were acquired via a diffusion-weighted echo-planar imaging sequence with the following parameters: repetition time/echo time (TR/TE), 10000/216 or 210 ms; field of view (FOV), 113 × 73.45 mm; matrix, 120 × 78; section thickness, 4 mm with no intersection gaps; voxel size, 3.55 mm^3; and number of averages, 1. The diffusion gradients were applied vertically to the table at a duration time (δ) of 79 or 80.8 ms, a separation time (Δ) of 101 or 98 ms, effective diffusion time ($\Delta_{eff} = \Delta - \delta/3$) of 74.7 or 71.1 ms, and 11 distinct gradient strengths (g mT/m). The resulting 11 b values were 0, 500, 1000, 2000, 3000, 4000, 5000, 6000, 7000, 8000, and 9000 s/mm^2, which corresponded to 11 q values of 0, 133, 189, 267, 327, 377, 422, 462, 499, 534, and 566 /cm, respectively. T2-weighted images (T2WIs) were acquired using a fast spin-echo sequence with the following parameters: TR/TE, 5000/91 ms; FOV, 87 × 43.5 mm; section thickness, 2 mm with a 1-mm intersection gap; matrix, 384 × 192; voxel size, 0.103 mm^3; averages, 10; turbo factor, 12; and parallel imaging factor, 2. We selected the 2-mm sections with a 1-mm gap and TE of 91 ms to obtain high-resolution T2WIs with a better signal-to-noise ratio, which were used as references to QSI maps. The acquisition time was 2 min 20 s for the QSI and 12 min 37 s for the T2WIs.

Image Processing

Based on the QSI procedure (23,24), the raw QSI data were evaluated using an in-house interactive data language program (25) with the algorithms described by Cohen and Assaf (24). In short, the q-space method was used to correlate the attenuation of the signal intensity (SI) of the diffusion measurements to the displacement probabilities through the reciprocal spatial vector q (defined as $\gamma\delta g/2\pi$),

in accordance with the following equation (20,21):

$$\overline{E_A}(q) = \int \overline{P_S}(R,\Delta)\exp(i2\pi qR)dR, \qquad [1]$$

where $\overline{E_A}(q)$ is the calculated SI decay as a function of q for a specific diffusion time

(Δ), $\overline{P_S}(R,\Delta)$ is the averaged diffusion propagator (displacement probability), and R

is the net displacement vector (R = r–r$_0$; r$_0$ is the initial spin position and r is the final

spin position after the time of Δ). Before Fourier transform, linear interpolation

between elements was performed, even though the data were not extrapolated. From

the equation [1], Fourier transform of the SI decay with respect to q was performed to

acquire the displacement distribution profiles based on the following equation:

$$\overline{P_S}(R,\Delta) = \int \overline{E_A}(q)\exp(-i2\pi qR)dq. \qquad [2]$$

Further details of the algorithms are reported elsewhere (23,24).

The three QSI parameters, mean displacement (MDP; μm), zero-displacement

probability (ZDP; arbitrary units [a.u.]), and kurtosis (K; a.u.), were calculated from

the displacement distribution profile of each voxel (23-25). Moments were calculated

from the propagator and applied to estimate the QSI parameters. The MDP value

was calculated as 0.425-fold of the full width at half maximum of the displacement

distribution profiles. The ZDP value was calculated as the height of the profiles at

zero displacement. The K value was calculated as the deviation form the Gaussian

distribution based on the following equation:

$$\text{Kurtosis} = \frac{1}{N}\sum_{j=0}^{N-1}\left(\frac{P_j - \overline{P}}{\sqrt{\text{Variance}}}\right)^4 - 3. \qquad [3]$$

Because of the linear interpolation between elements, a greater number of elements

was used to calculate the K value, as opposed to the actual number of samples, thus

the K values in the present study were relatively larger. The interpolation in q-space

led to longer tails of the displacement distribution profiles acquired by Fourier

transform. Therefore, the extended tails of the displacement distribution profiles likely

led to added deviation form the Gaussian distribution, which resulted in greater K

values, as K is a deviation from the Gaussian distribution (26). Then, MDP, ZDP, and

K maps were generated based on these three parameters on a voxel-by-voxel basis.

Also, the apparent diffusion coefficient (ADC) was calculated for each voxel based on

the following equation:

$$ADC = - \ln(S/S_0)/(b-b_0), \qquad\qquad\qquad [4]$$

where b_0 is 0 s/mm^2, b is 500 s/mm^2, and S_0 and S are the SI at the b_0 and b values, respectively. ADC maps were also generated on a voxel-by-voxel basis.

Image Analysis

Two observers (I.Y., N.Y.; with 26 and 23 years of experience in reading MR images, respectively), blinded to the histopathologic findings, had independently evaluated the MR images of each surgical specimen. Disagreements in any finding were resolved via discussion and consensus. For each sample, the CRC contour and SI were analyzed, and the depth of tumor penetration was calculated based on the deepest point of invasion. The size, SI, and border contour of the resected LNs were also calculated using the MR images. The MRI and histopathologic findings were compared on a node-by-node basis. The T2WIs were not obtained for the resected LNs, and thus the sensitivity and specificity of the T2WIs for detecting LNM were not evaluated in this study.

For the MDP, ZDP, K, and ADC maps, each region of interest (ROI), which was approximately equal to the size of the cross-sectional area of the tumor or LN, was drawn on the CRC and resected LNs by a single observer with the T2WIs and diffusion-weighted images as references. After placing three or four ROIs over the tumor and LNs, ImageJ 1.47 software (https://imagej.nih.gov/) was used to calculate the mean values of all ROIs for each tumor and LN to generate quantitative data. Finally, the MRI findings of all tissue samples were compared with the corresponding histopathologic findings on a slice-by-slice level by visual and spatial matching based on anatomic features, which included the blood vessels and contour details.

Histologic Preparation and Examination

After QSI, each specimen was sectioned along the longitudinal axis to ensure correspondence between the MR images and histologic sections. The sections were embedded in paraffin, sectioned into 6-μm-thick slices with a microtome, and then stained with hematoxylin-eosin, elastica-van Gieson, and periodic acid-Schiff. A single experienced pathologist, blinded to the MRI results, evaluated all tissue samples to determine the extent of tumor invasion into the colorectal wall. Afterward, the HG was classified as well-differentiated (WD), moderately differentiated (MD), or poorly differentiated (PD), based on the American Joint Committee on Cancer

guidelines (1,2), and the extent of LNM was determined. The pathologist examined all the sections through the LNs and individually evaluated all resected LNs for the presence of tumor, where LNs that had tumor cells were considered positive for LNM and isolated tumor cells (cell deposits less than or equal to 0.2 mm) were also considered positive.

Statistical Analysis

The mean ± standard deviation (SD) of the MDP, ZDP, K, and ADC values of the tumors and LNs were calculated from the corresponding maps. All analyses were conducted using IBM SPSS Statistics, version 20.0 (IBM SPSS Japan, Tokyo, Japan). The Spearman's rank correlation coefficient was used to identify correlations between the HG and QSI parameters. The Mann-Whitney U-test was used to compare the QSI parameters of the metastatic and non-metastatic LNs.

Receiver operating characteristic (ROC) curve analyses using the area under the curve (AUC) were conducted to evaluate and compare the MDP, ZDP, K, and ADC values in terms of usefulness to discriminate the HG of CRC and to discern metastatic from non-metastatic LNs. The optimal threshold of each parameter was determined as the value with the highest average of sensitivity and specificity. A probability (P) value of < 0.05 was considered statistically significant.

Results

MDP, ZDP, K, and ADC Values of CRC

Histopathologic assessment of the 20 CRC tissue samples revealed that invasion into the colorectal wall was the submucosa in three cases (stage T1), the muscularis propria in three cases (stage T2), the subserosa in 10 cases (stage T3), and the serosa in four cases (stage T4).

For all 20 CRCs, the mean MDP, ZDP, K, and ADC values were 8.87 ± 0.37 μm, 82.0 ± 6.2 a.u., 74.3 ± 3.0 a.u., and $0.219 ± 0.040 × 10^{-3}$ mm^2/s, respectively. The K value is a measure of the degree of deviation from a Gaussian distribution, where a K value of 3 indicates a perfect Gaussian diffusion (23-26). Hence, the greater the K value, the greater deviation from a perfect Gaussian diffusion. Meanwhile, the ADC value is calculated based on the notion that water diffusion follows a Gaussian behavior.

HG of CRC based on QSI Maps

The association between the HG of the CRC and the non-Gaussian QSI parameters was investigated. Histopathologic examination of the 20 CRC tissue samples revealed that six were WD, 13 were MD, and one was PD. As shown in Table 1 and Figure 2, comparisons of the QSI parameters with the HGs of the 20 CRCs revealed significant correlations between the MDP, ZDP, and K values and the HGs of the CRCs (r = −0.768, P < 0.001; r = 0.768, P < 0.001; and r = 0.785, P < 0.001, respectively). However, no significant correlation was found between the ADC values and the HGs of the CRCs (r = 0.088, P = 0.712).

A representative case with MD CRC is shown in Figure 3. These findings clarified that it is possible to discriminate the HG of CRC on the basis of non-Gaussian QSI parameters (Figure 4).

Extent of LNM based on QSI Maps

LNM was identified in 8 (40%) of 20 cases and each histologically confirmed LN (8 metastatic and 12 non-metastatic) was compared with the QSI parameters on a node-by-node basis. We used only the largest LN among the resected LNs for each subject to avoid repeated-measurement (clustering) bias. As shown in Table 2 and Figure 5, the MDP values of the metastatic LNs were significantly less than those of the non-metastatic LNs, while the ZDP and K values were significantly greater (all, P < 0.001). However, there were no significant differences between the ADC values of the metastatic and non-metastatic LNs (P = 0.082).

A representative case with metastatic LNs is shown in Figures 6. These findings indicated that it is possible to discriminate between metastatic and non-metastatic LNs in CRC on the basis of non-Gaussian QSI parameters (Figure 7).

ROC Curve Analyses of the MDP, ZDP, K, and ADC Values

As shown in Table 3 and Figure 8a, to differentiate MD or PD from WD CRC, the AUCs for the MDP, ZDP, and K values (0.952, P = 0.0104; 0.952, P = 0.0060; and 0.964, P = 0.0057, respectively) were significantly greater than for the ADC values (0.583), while there were no significant differences among the MDP, ZDP, and K values (P = 0.7014−1.0000). So, MDP, ZDP, and K cutoff values of ≤ 8.797 μm, > 82.652 a.u., and > 73.006 a.u. seemed to be useful to differentiate MD or PD from WD CRC.

As shown in Table 4 and Figure 8b, to differentiate between metastatic and non-metastatic LNs in CRC, the AUCs for the MDP, ZDP, and K values (0.990, P = 0.0217; 0.969, P = 0.0192; and 0.990, P = 0.0217, respectively) were significantly greater than for the ADC values (0.740), while there were no significant differences among the MDP, ZDP, and K values (P = 0.4028−1.0000). So, MDP, ZDP, and K cutoff values of ≤ 14.768 μm, > 29.349 a.u., and > 29.503 a.u. seemed to be useful to differentiate metastatic from non-metastatic LNs in CRC.

Discussion

Assaf et al. (23) first described QSI as a non-Gaussian diffusion-weighted imaging (DWI) method for evaluation of the spinal cord and to quantify the deviation of tissue diffusion from Gaussian behavior in tissues with restricted water diffusion. As compared with conventional DWI, QSI more accurately reflects the microstructural complexity of tissues (23,27,28). More recently, Yamada et al. (20,21) reported that QSI was useful for ex vivo evaluation of the HG and extent of LNM in esophageal and gastric carcinomas. Therefore, we postulated that QSI is more efficient than conventional DWI for evaluation of the HG and extent of LNM in CRC.

In the present study, the mean MDP, ZDP, K, and ADC values were derived from the QSI data of all the CRC cases. Previous studies (23-26) have reported that the MDP value quantitatively reflects the architecture size of tissues and is decreased in tissues that have more restricted diffusivity. The ZDP value reflects the fraction of water molecules that diffuse a short distance or not at all and is increased in tissues with more restricted diffusivity. The K value reflects the degree of deviation from the Gaussian distribution in water diffusion. Since a K value of 3 indicates a perfect Gaussian diffusion (23-26), the greater the K value, the greater deviation from a perfect Gaussian diffusion. These findings confirmed the substantial contribution of the effect of non-Gaussian diffusion to the QSI parameters of CRC. These propensities were in accordance with the results of prior studies of other organs (20,21).

The results of the present study revealed significant associations between the QSI parameters and HG of CRC. Other studies have reported associations between diffusional kurtosis acquired by diffusion kurtosis imaging (DKI) of cerebral gliomas and prostate cancers and the HG of the tumors (29,30), suggesting that diffusional

kurtosis calculated by DKI increases with tumor aggressiveness because of the greater microstructural complexity of high-grade tumors (30). Since QSI is very sensitive to changes in tissue microstructure (23,27,28), QSI may be an efficient method to noninvasively evaluate the HG of CRC. Prior studies have reported that it is often problematic to discriminate between the HGs of tumor based only on ADC values because of the sizable overlap between the ADC values of different HGs of tumor (31-33). Thus, QSI may be a more accurate method than conventional DWI to discern the HG of CRC.

In the present study, ROC curve analyses to discriminate the HG of CRC confirmed that the AUCs for the MDP, ZDP, and K values were significantly greater than for the ADC values. Moreover, the MDP, ZDP, and K cutoff values were useful to discriminate MD or PD from WD CRC, as compared with conventional ADC values.

QSI was also useful to discriminate between metastatic and non-metastatic LNs in CRC. Prior studies have reported that the assessment of LNs in CRC by any imaging modality is difficult because LN size alone is not a consistent diagnostic criterion of metastatic involvement (9,34). Other studies have demonstrated that although ADC values may be valuable to identify metastatic LNs, it is often problematic to discriminate between metastatic and non-metastatic LNs on the basis of ADC values alone because of the considerable overlap between the ADC values of metastatic and non-metastatic LNs (35-38). Based on the ability to predict microstructural complexity, QSI may be a useful tool for noninvasive evaluation of the extent of LNM in CRC.

ROC curve analyses to discriminate between metastatic and non-metastatic LNs in CRC demonstrated that the AUCs of the MDP, ZDP, and K values were significantly greater than the AUC of ADC values. Furthermore, the MDP, ZDP, and K cutoff values were useful to discriminate metastatic from non-metastatic LNs in CRC, as compared with the ADC values.

Conventional MRI has reportedly been used to stage CRC before surgery using multichannel phased-array coils, parallel imaging methods, and more powerful gradient systems (10-15). Moreover, endoluminal MRI with endoluminal coils has been used for staging of rectal carcinomas (16-19). Hence, these novel techniques will allow the performance of QSI for preoperative evaluation of CRC.

There were several limitations to this study that should be addressed. First, this was an ex vivo study of tissue samples that were imaged after fixation in formalin.

Nevertheless, prior studies of other organs revealed that even though the ADC values of fixed tissues were relatively low, the differences in ADC values among various tissue types in vivo were maintained in the fixed tissues. Thus, these differences in relative ADC values between fixed and in vivo tissues were not statistically significant (39,40). Hence, the data acquired in the present study can be applied to QSI of tissues in vivo as well as formalin-fixed.

As a second limitation, the QSI protocol required a slightly longer period of time to complete (2 min 20 s), which may prohibit use in clinical practice. Therefore, the imaging time must be decreased for application of in vivo QSI. The direct clinical application of QSI for evaluation of CRC may be technically problematic because of motion effects (peristalsis, respiratory movements, and patient motion) and the deep abdominal location of the colon and rectum. Adjustments to the pulse sequences, improvement to the duration of the MRI technique, and application of greater field strengths may be needed to improve the technical feasibility of this technique in clinical settings.

A third limitation was the relatively limited number of tissue samples for examination which questions reproducibility. To address this limitation, we plan to collect colorectal further QSI data with an ultimate goal of routine application of QSI as a quantitative tool for accurate evaluation of CRC before surgery to select an optimal therapy.

In conclusion, the ex vivo QSI-derived MDP, ZDP, and K values showed significant correlations with the HG of CRC and revealed significant differences between metastatic and non-metastatic LNs in CRC. Therefore, the results of this study demonstrated that QSI ex vivo provides useful diagnostic information to evaluate the HG and extent of LNM in CRC.

References

1. Lan YT, Yang SH, Chang SC, et al. Analysis of the seventh edition of American Joint Committee on colon cancer staging. Int J Colorectal Dis 2012;27:657-663.

2. Gao P, Song YX, Wang ZN, et al. Is the prediction of prognosis not improved by the seventh edition of the TNM classification for colorectal cancer? Analysis of the surveillance, epidemiology, and end results (SEER) database. BMC Cancer 2013;13:123.

3. Sibileau E, Ridereau-Zins C, Vanel D, et al. Accuracy of water-enema multidetector computed tomography (WE-MDCT) in colon cancer staging: a prospective study. Abdom Imaging 2014;39:941-948.

4. Soyer P, Hamzi L, Sirol M, et al. Colon cancer: comprehensive evaluation with 64-section CT colonography using water enema as intraluminal contrast agent-a pictorial review. Clin Imaging 2012;36:113-125.

5. Mondal D, Betts M, Cunningham C, Mortensen NJ, Lindsey I, Slater A. How useful is endorectal ultrasound in the management of early rectal carcinoma? Int J Colorectal Dis 2014;29:1101-1104.

6. Colaiacovo R, Assef MS, Ganc RL, et al. Rectal cancer staging: Correlation between the evaluation with radial echoendoscope and rigid linear probe. Endosc Ultrasound 2014;3:161-166.

7. Ahuja NK, Sauer BG, Wang AY, et al. Performance of endoscopic ultrasound in staging rectal adenocarcinoma appropriate for primary surgical resection. Clin Gastroenterol Hepatol 2015;13:339-344.

8. Yamada I, Okabe S, Enomoto M, et al. Colorectal carcinoma: in vitro evaluation with high-spatial-resolution 3D constructive interference in steady-state MR imaging. Radiology 2008;246:444-453.

9. Yamada I, Yoshino N, Tetsumura A, et al. Colorectal Carcinoma: Local Tumor Staging and Assessment of Lymph Node Metastasis by High-Resolution MR Imaging in Surgical Specimens. Int J Biomed Imaging 2009;2009:659836.

10. Sprouse T, Jensen CT, Vicens R, Ernst R, Bhosale P. Local magnetic resonance imaging staging of rectal adenocarcinoma. J Comput Assist Tomogr 2014;38:885-889.

11. Patel RK, Sayers AE, Kumar P, Khulusi S, Razack A, Hunter IA. The role of endorectal ultrasound and magnetic resonance imaging in the management of early

rectal lesions in a tertiary center. Clin Colorectal Cancer 2014;13:245-250.

12. Keane C, Young M. Accuracy of magnetic resonance imaging for preoperative staging of rectal cancer. ANZ J Surg 2014;84:758-762.

13. Gowdra Halappa V, Corona Villalobos CP, Bonekamp S, et al. Rectal imaging: part 1, High-resolution MRI of carcinoma of the rectum at 3 T. AJR Am J Roentgenol 2012;199:W35-42.

14. Sani F, Foresti M, Parmiggiani A, et al. 3-T MRI with phased-array surface coil in the local staging of rectal cancer. Radiol Med 2011;116:375-388.

15. Kim H, Lim JS, Choi JY, et al. Rectal cancer: comparison of accuracy of local-regional staging with two- and three-dimensional preoperative 3-T MR imaging. Radiology 2010;254:485-492.

16. Wong EM, Leung JL, Cheng CS, Lee JC, Li MK, Chung CC. Effect of endorectal coils on staging of rectal cancers by magnetic resonance imaging. Hong Kong Med J 2010;16:421-426.

17. Tamakawa M, Kawaai Y, Shirase R, et al. Gadolinium-enhanced dynamic magnetic resonance imaging with endorectal coil for local staging of rectal cancer. Jpn J Radiol 2010;28:290-298.

18. Donmez FY, Tunaci M, Yekeler E, Balik E, Tunaci A, Acunas G. Effect of using endorectal coil in preoperative staging of rectal carcinomas by pelvic MR imaging. Eur J Radiol 2008;67:139-145.

19. Tatli S, Mortele KJ, Breen EL, Bleday R, Silverman SG. Local staging of rectal cancer using combined pelvic phased-array and endorectal coil MRI. J Magn Reson Imaging 2006;23:534-540.

20. Yamada I, Hikishima K, Miyasaka N, et al. Esophageal carcinoma: Evaluation with q-space diffusion-weighted MR imaging ex vivo. Magn Reson Med 2015;73:2262-2273.

21. Yamada I, Hikishima K, Miyasaka N, et al. q-space MR imaging of gastric carcinoma ex vivo: Correlation with histopathologic findings. Magn Reson Med 2016;76:602-612.

22. Yamada I, Yoshino N, Hikishima K, et al. Colorectal carcinoma: Ex vivo evaluation using 3-T high-spatial-resolution quantitative T2 mapping and its correlation with histopathologic findings. Magn Reson Imaging 2017;38:174-181.

23. Assaf Y, Mayk A, Cohen Y. Displacement imaging of spinal cord using q-space diffusion-weighted MRI. Magn Reson Med 2000;44:713-722.

24. Cohen Y, Assaf Y. High b-value q-space analyzed diffusion-weighted MRS and MRI in neuronal tissues - a technical review. NMR Biomed 2002;15:516-542.

25. Hikishima K, Yagi K, Numano T, et al. Volumetric q-space imaging by 3D diffusion-weighted MRI. Magn Reson Imaging 2008;26:437-445.

26. Ong HH, Wright AC, Wehrli SL, et al. Indirect measurement of regional axon diameter in excised mouse spinal cord with q-space imaging: simulation and experimental studies. Neuroimage 2008;40:1619-1632.

27. Bar-Shir A, Duncan ID, Cohen Y. QSI and DTI of excised brains of the myelin-deficient rat. Neuroimage 2009;48:109-116.

28. Anaby D, Duncan ID, Smith CM, Cohen Y. White matter maturation in the brains of Long Evans shaker myelin mutant rats by ex-vivo QSI and DTI. Magn Reson Imaging 2013;31:1097-1104.

29. Raab P, Hattingen E, Franz K, Zanella FE, Lanfermann H. Cerebral gliomas: diffusional kurtosis imaging analysis of microstructural differences. Radiology 2010;254:876-881.

30. Rosenkrantz AB, Sigmund EE, Johnson G, et al. Prostate cancer: feasibility and preliminary experience of a diffusional kurtosis model for detection and assessment of aggressiveness of peripheral zone cancer. Radiology 2012;264:126-135.

31. Sugahara T, Korogi Y, Kochi M, et al. Usefulness of diffusion-weighted MRI with echo-planar technique in the evaluation of cellularity in gliomas. J Magn Reson Imaging 1999;9:53-60.

32. Kono K, Inoue Y, Nakayama K, et al. The role of diffusion-weighted imaging in patients with brain tumors. AJNR Am J Neuroradiol 2001;22:1081-1088.

33. Koral K, Mathis D, Gimi B, et al. Common pediatric cerebellar tumors: correlation between cell densities and apparent diffusion coefficient metrics. Radiology 2013;268:532-537.

34. Ogawa S, Hida J, Ike H, et al. The important risk factor for lateral pelvic lymph node metastasis of lower rectal cancer is node-positive status on magnetic resonance imaging: study of the Lymph Node Committee of Japanese Society for Cancer of the Colon and Rectum. Int J Colorectal Dis 2016;31:1719-1728.

35. Sumi M, Sakihama N, Sumi T, et al. Discrimination of metastatic cervical lymph nodes with diffusion-weighted MR imaging in patients with head and neck cancer. AJNR Am J Neuroradiol 2003;24:1627-1634.

36. King AD, Ahuja AT, Yeung DK, et al. Malignant cervical lymphadenopathy:

diagnostic accuracy of diffusion-weighted MR imaging. Radiology 2007;245:806-813.

37. Vandecaveye V, De Keyzer F, Vander Poorten V, et al. Head and neck squamous cell carcinoma: value of diffusion-weighted MR imaging for nodal staging. Radiology 2009;251:134-146.

38. Wu LM, Xu JR, Hua J, Gu HY, Zhu J, Hu J. Value of diffusion-weighted MR imaging performed with quantitative apparent diffusion coefficient values for cervical lymphadenopathy. J Magn Reson Imaging 2013;38:663-670.

39. Xu J, Humphrey PA, Kibel AS, et al. Magnetic resonance diffusion characteristics of histologically defined prostate cancer in humans. Magn Reson Med 2009;61:842-850.

40. Bourne R, Kurniawan N, Cowin G, Sved P, Watson G. 16 T diffusion microimaging of fixed prostate tissue: preliminary findings. Magn Reson Med 2011;66:244-247.

TABLE 1. MDP, ZDP, K, and ADC Values of the Different Histologic Grades of the Colorectal Carcinomas

Histologic Grades	MDP (μm)	ZDP (a.u.)	K (a.u.)	ADC (x 10^{-3} mm^2/sec)
WD (n = 6)	9.25 ± 0.28*	75.2 ± 4.6*	70.9 ± 1.8*	0.214 ± 0.035
MD (n = 13)	8.75 ± 0.19	84.3 ± 3.7	75.4 ± 1.7	0.222 ± 0.045
PD (n = 1)	8.07	92.8	80.3	0.209

Note: WD = Well-differentiated, MD = Moderately differentiated, PD = Poorly differentiated. a.u. = arbitrary units. * = Significantly different for the different histologic grades of the colorectal carcinomas (P < 0.001).

TABLE 2. MDP, ZDP, K, and ADC Values of the Metastatic and Non-metastatic Lymph Nodes of the Colorectal Carcinomas

Lymph Nodes	MDP (µm)	ZDP (a.u.)	K (a.u.)	ADC (x 10^{-3} mm^2/sec)
Non-metastatic (n = 12)	18.6 ± 2.3*	27.3 ± 4.5*	26.8 ± 5.5*	0.274 ± 0.035
Metastatic (n = 8)	10.9 ± 1.9	51.9 ± 13.1	58.7 ± 10.5	0.243 ± 0.041

Note.-- a.u. = arbitrary units. * = Significantly different between the metastatic and non-metastatic lymph nodes of the colorectal carcinomas ($P < 0.001$).

TABLE 3. ROC Curve Analyses of MDP, ZDP, K, and ADC Values for Differentiating MD or PD from WD Colorectal Carcinomas

Parameter	AUC	Optimal Threshold	Sensitivity (%)	Specificity (%)	P Value
MDP	0.952	≤ 8.797 (µm)	85.7 (12/14)	100.0 (6/6)	0.0104
ZDP	0.952	> 82.652 (a.u.)	78.6 (11/14)	100.0 (6/6)	0.0060
K	0.964	> 73.006 (a.u.)	92.9 (13/14)	100.0 (6/6)	0.0057
ADC	0.583	> 0.252 ($\times 10^{-3}$ mm^2/s)	28.6 (4/14)	100.0 (6/6)	NA

Note: Optimal threshold of each parameter was determined to maximize average of sensitivity and specificity. Data in parentheses are numbers used to calculate percentages. P value represents differences in comparison with performance of ADC. WD = Well-differentiated, MD = Moderately differentiated, PD = Poorly differentiated. AUC = area under the curve. a.u. = arbitrary units. NA = not available.

TABLE 4. ROC Curve Analyses of MDP, ZDP, K, and ADC Values for Differentiating Metastatic from Non-metastatic Lymph Nodes in Colorectal Carcinoma

Parameter	AUC	Optimal Threshold	Sensitivity (%)	Specificity (%)	P Value
MDP	0.990	≤ 14.768 (µm)	100.0 (8/8)	91.7 (11/12)	0.0217
ZDP	0.969	> 29.349 (a.u.)	100.0 (8/8)	91.7 (11/12)	0.0192
K	0.990	> 29.503 (a.u.)	100.0 (8/8)	91.7 (11/12)	0.0217
ADC	0.740	≤ 0.282 ($\times 10^{-3}$ mm^2/s)	100.0 (8/8)	50.0 (6/12)	NA

Note: Optimal threshold of each parameter was determined to maximize average of sensitivity and specificity. Data in parentheses are numbers used to calculate percentages. P value represents differences in comparison with performance of ADC. AUC = area under the curve. a.u. = arbitrary units. NA = not available.

CAPTIONS FOR ILLUSTRATIONS

FIGURE 1: The surface coil, container, and small flasks used for imaging CRC.

a: The four-channel phased-array surface coil used for imaging the colorectal specimen and resected LNs.

b: The container and small flasks used for imaging the resected LNs.
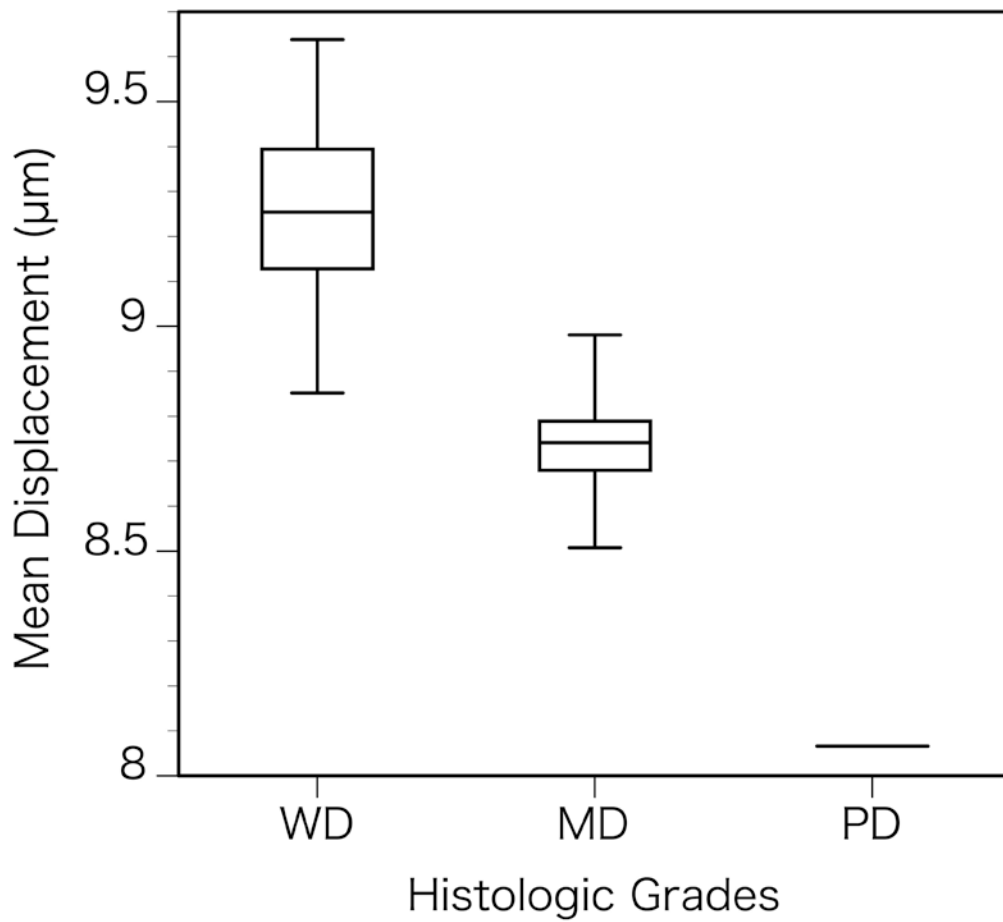
FIGURE 2: Box plots of the QSI parameters in the different HGs of CRCs.

a: Comparison of the MDP values in the different HGs of CRCs showing a significant inverse correlation (r = −0.768; P < 0.001).
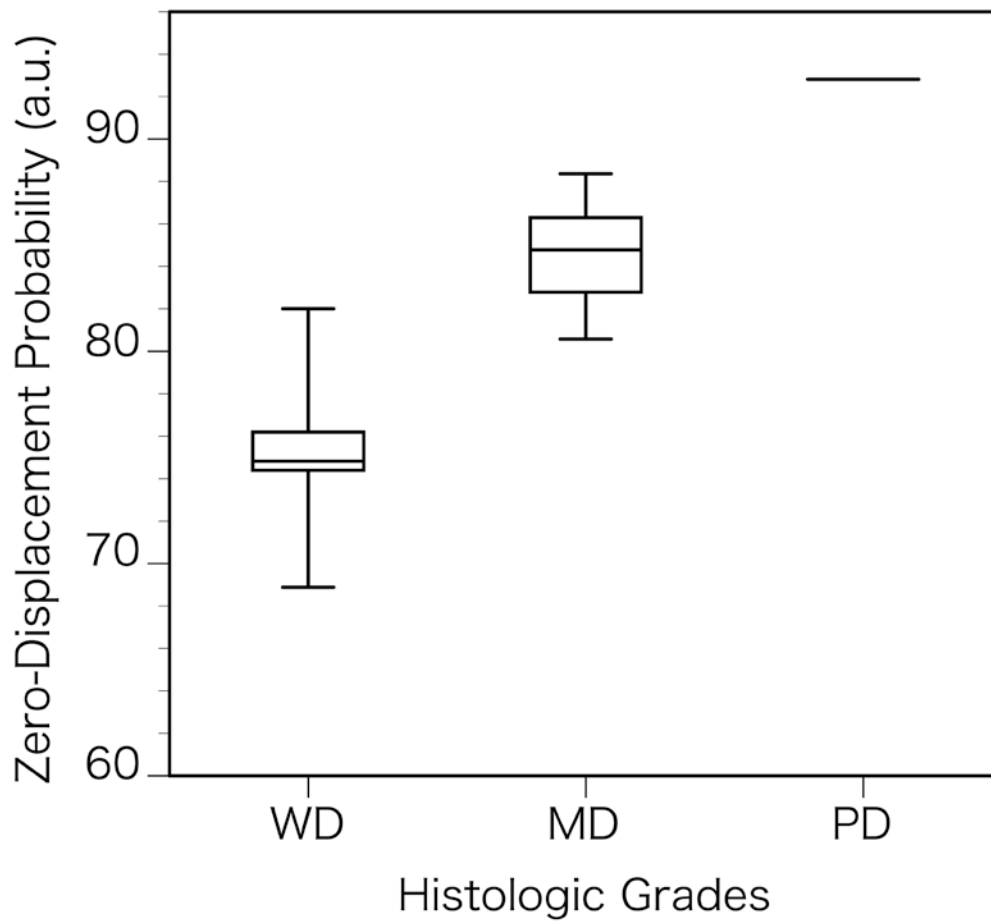
b: Comparison of the ZDP values in the different HGs of CRCs showing a significant positive correlation (r = 0.768; P < 0.001). (a.u. = arbitrary units.)

c: Comparison of the K values in the different HGs of CRCs also showing a significant positive correlation (r = 0.785; P < 0.001). (a.u. = arbitrary units.)

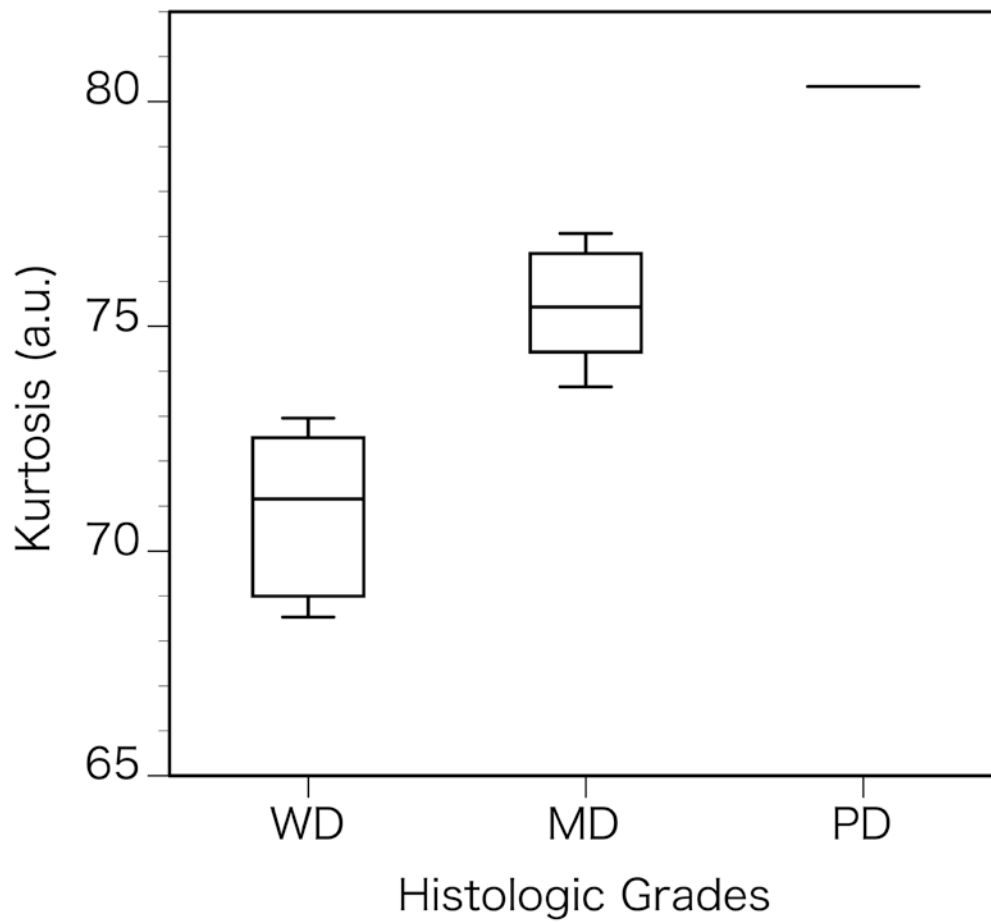**d:** Comparison of the ADC values in the different HGs of CRCs showing no significant correlation (r = 0.088; P = 0.712).

FIGURE 3: Images of a case with MD CRC invading the serosa (stage T4).

a: T2WI shows a hyperintense, irregular-shaped mass lesion (arrows) in the rectum.

b: MDP map shows that the mass lesion (arrows) is slightly hypointense (MDP = 8.74 μm).

c: ZDP map shows that mass lesion (arrows) is slightly hyperintense (ZDP = 84.8 a.u.).

d: K map shows that mass lesion (arrows) is slightly hyperintense (K = 75.4 a.u.).

FIGURE 4: Histopathologic sections of the CRCs.

a: Histopathologic section of a WD CRC. (Hematoxylin-eosin stain; original magnification, x200.)

b: Histopathologic section of an MD CRC. (Hematoxylin-eosin stain; original magnification, x200.)

c: Histopathologic section of a PD CRC. (Hematoxylin-eosin stain; original magnification, x200.)

FIGURE 5: Box plots of the QSI parameters in metastatic and non-metastatic LNs in

21

CRC.

a: The MDP values of the metastatic LNs were significantly less than those of the non-metastatic LNs (P < 0.001).

b: The ZDP values of the metastatic LNs were significantly greater than those of the non-metastatic LNs (P < 0.001). (a.u. = arbitrary units.)

c: The K values of the metastatic LNs were also significantly greater than those of the non-metastatic LNs (P < 0.001). (a.u. = arbitrary units.)

d: There were no significant differences between the ADC values of the metastatic and non-metastatic LNs (P = 0.082).

FIGURE 6: Images of a case with metastatic LNs in CRC.

a: DWI (b = 2000 s/mm^2) shows hyperintense, swollen LNs (arrow) in CRC.

b: MDP map shows the LNs (arrow) are slightly hypointense (MDP = 10.4 µm).

c: ZDP map shows that the LNs (arrow) are slightly hyperintense (ZDP = 52.7 a.u.).

d: K map shows that the LNs (arrow) are slightly hyperintense (K = 60.0 a.u.).

FIGURE 7: Histopathologic sections of non-metastatic and metastatic LNs in CRC.

a: Histopathologic section of a non-metastatic LN. (Hematoxylin-eosin stain; original magnification, x40.)

b: Histopathologic section of a metastatic LN. (Hematoxylin-eosin stain; original magnification, x40.)

FIGURE 8: ROC curve analyses of the QSI parameters in CRC.

a: ROC curves for differentiating MD or PD from WD CRC. The AUCs for the MDP, ZDP, and K values (0.952, P = 0.0104; 0.952, P = 0.0060; and 0.964, P = 0.0057, respectively) were significantly greater than for the ADC values (0.583). There were no significant differences among the MDP, ZDP, and K values (P = 0.7014−1.0000).

b: ROC curves for differentiating metastatic from non-metastatic LNs in CRC. The AUCs for the MDP, ZDP, and K values (0.990, P = 0.0217; 0.969, P = 0.0192; and 0.990, P = 0.0217, respectively) were significantly greater than for the ADC values (0.740). There were no significant differences among the MDP, ZDP, and K values (P = 0.4028−1.0000).

FIGURE 1: The surface coil, container, and small flasks used for imaging CRC.
a: The four-channel phased-array surface coil used for imaging the colorectal specimen and resected LNs.

FIGURE 1: The surface coil, container, and small flasks used for imaging CRC.
b: The container and small flasks used for imaging the resected LNs.

FIGURE 2: Box plots of the QSI parameters in the different HGs of CRCs.

a: Comparison of the MDP values in the different HGs of CRCs showing a significant inverse correlation (r = −0.768; P < 0.001).

FIGURE 2: Box plots of the QSI parameters in the different HGs of CRCs.

b: Comparison of the ZDP values in the different HGs of CRCs showing a significant positive correlation (r = 0.768; P < 0.001). (a.u. = arbitrary units.)

FIGURE 2: Box plots of the QSI parameters in the different HGs of CRCs.
c: Comparison of the K values in the different HGs of CRCs also showing a significant positive correlation (r = 0.785; P < 0.001). (a.u. = arbitrary units.)
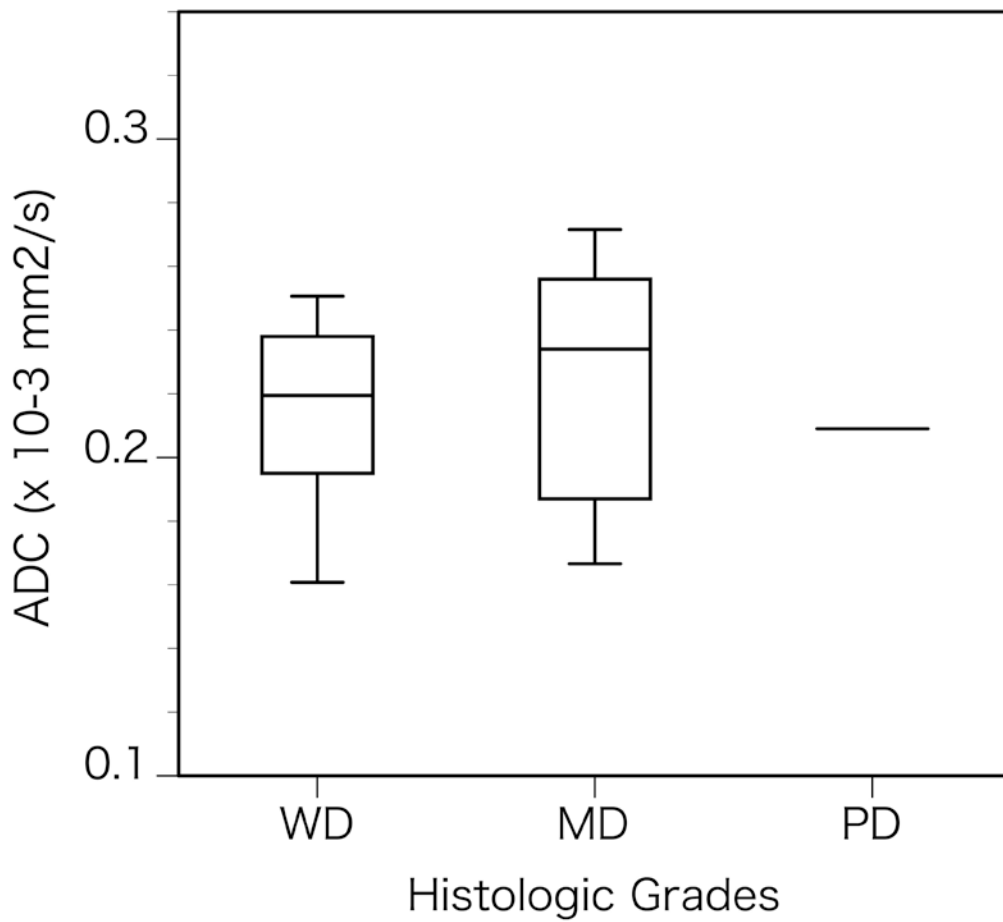
FIGURE 2: Box plots of the QSI parameters in the different HGs of CRCs.
d: Comparison of the ADC values in the different HGs of CRCs showing no significant correlation (r = 0.088; P = 0.712).
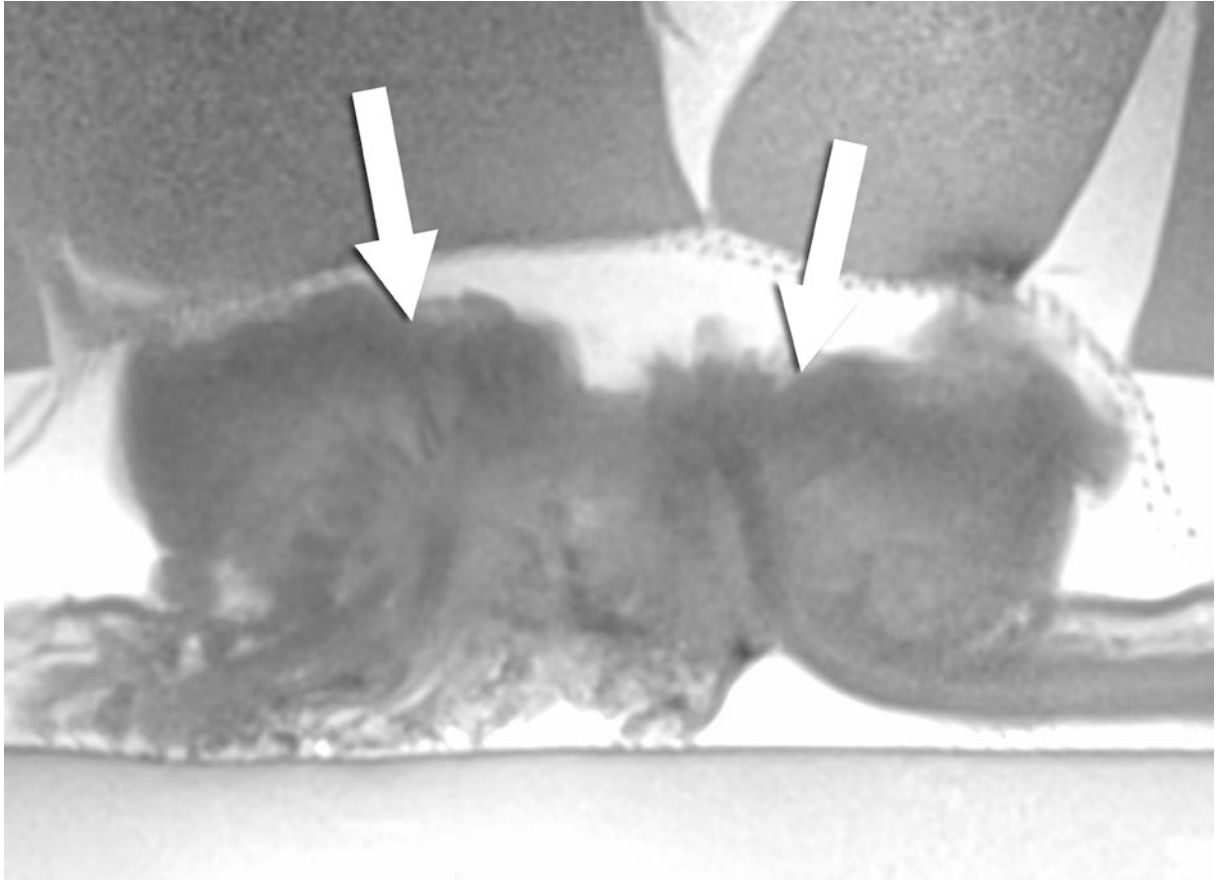
FIGURE 3: Images of a case with MD CRC invading the serosa (stage T4).

a: T2WI shows a hyperintense, irregular-shaped mass lesion (arrows) in the rectum.
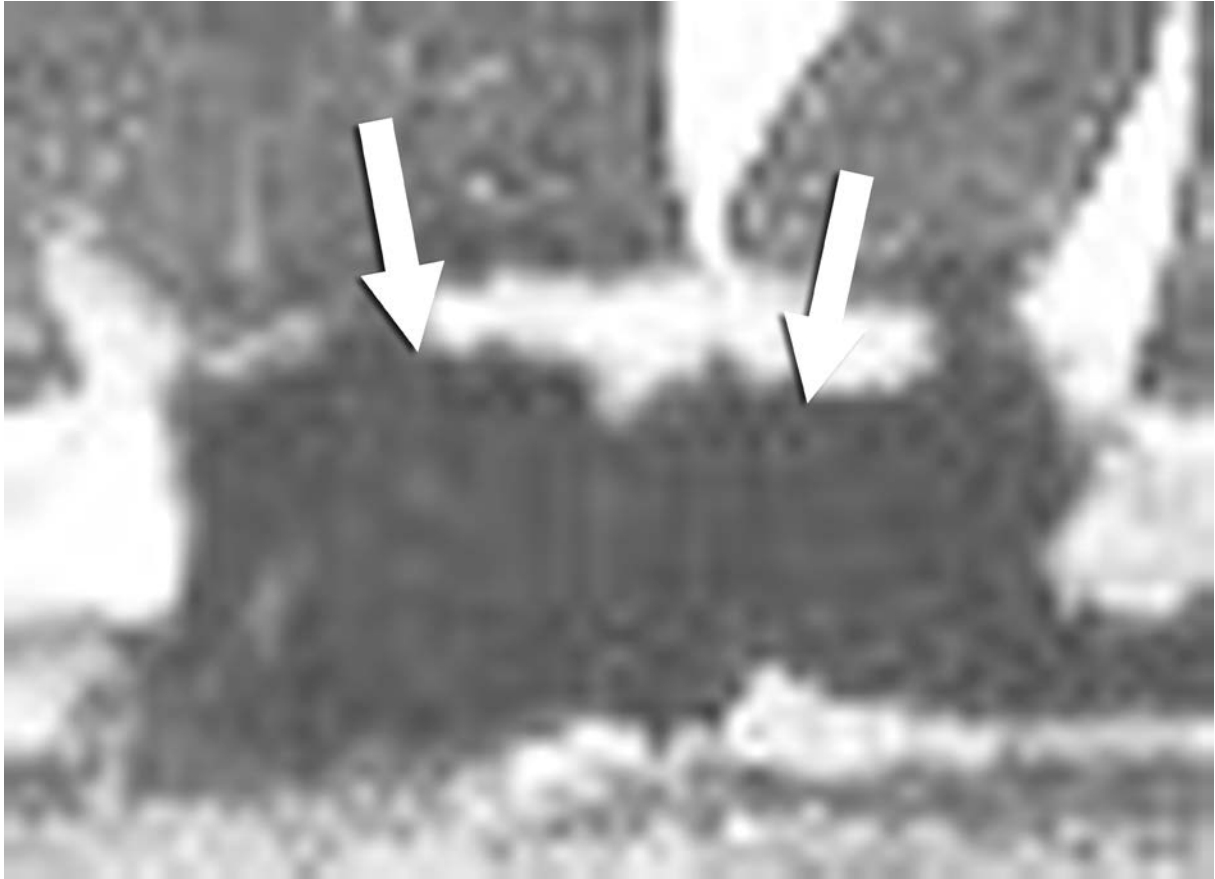
FIGURE 3: Images of a case with MD CRC invading the serosa (stage T4).

b: MDP map shows that the mass lesion (arrows) is slightly hypointense (MDP = 8.74 μm).
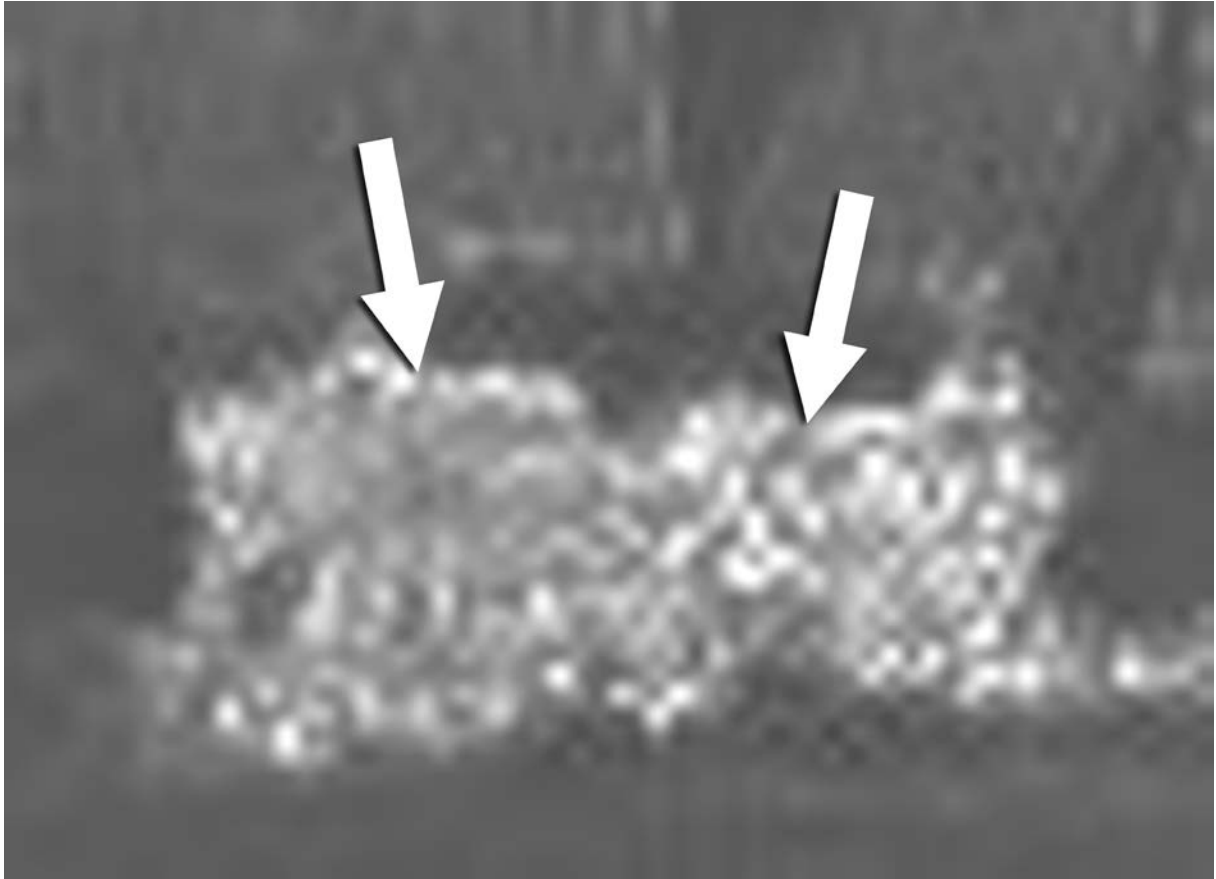
FIGURE 3: Images of a case with MD CRC invading the serosa (stage T4).

c: ZDP map shows that mass lesion (arrows) is slightly hyperintense (ZDP = 84.8 a.u.).
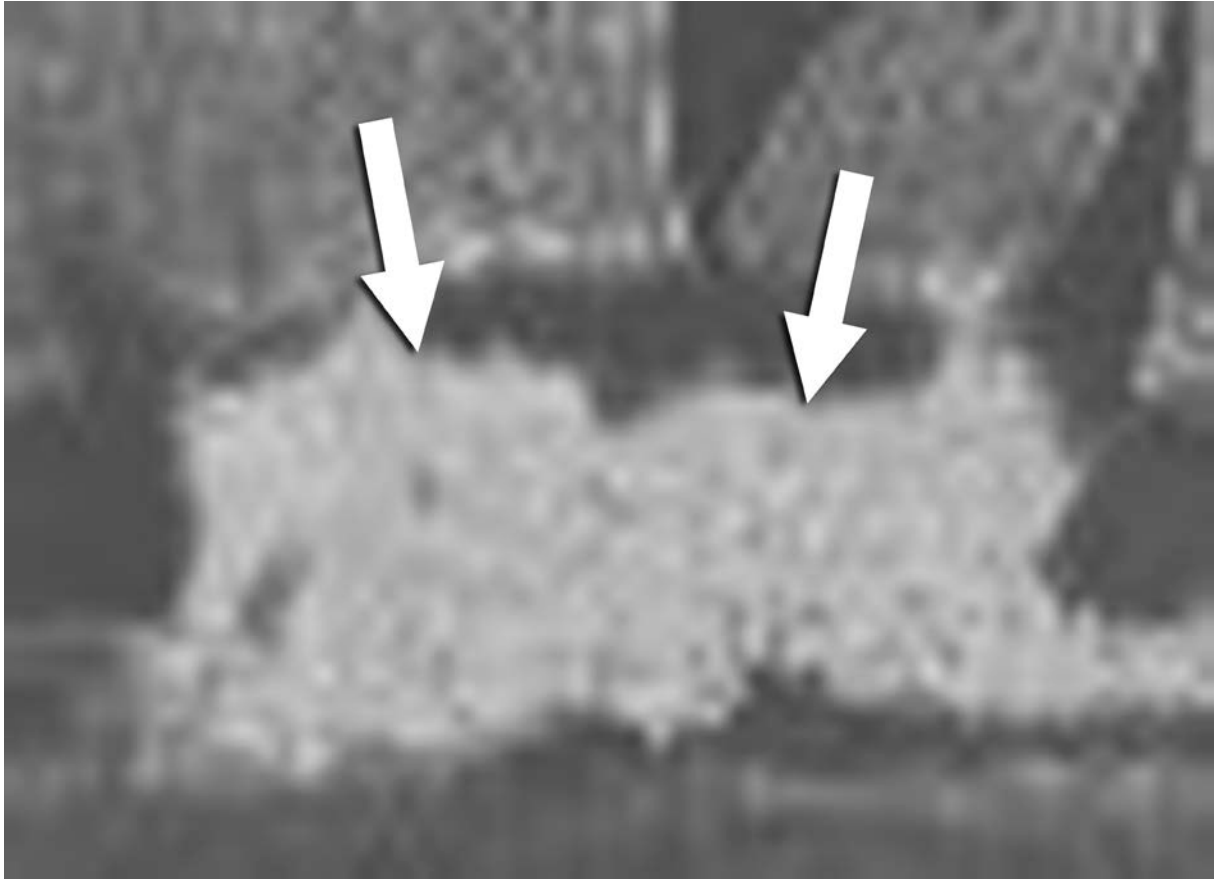
FIGURE 3: Images of a case with MD CRC invading the serosa (stage T4).

d: K map shows that mass lesion (arrows) is slightly hyperintense (K = 75.4 a.u.).
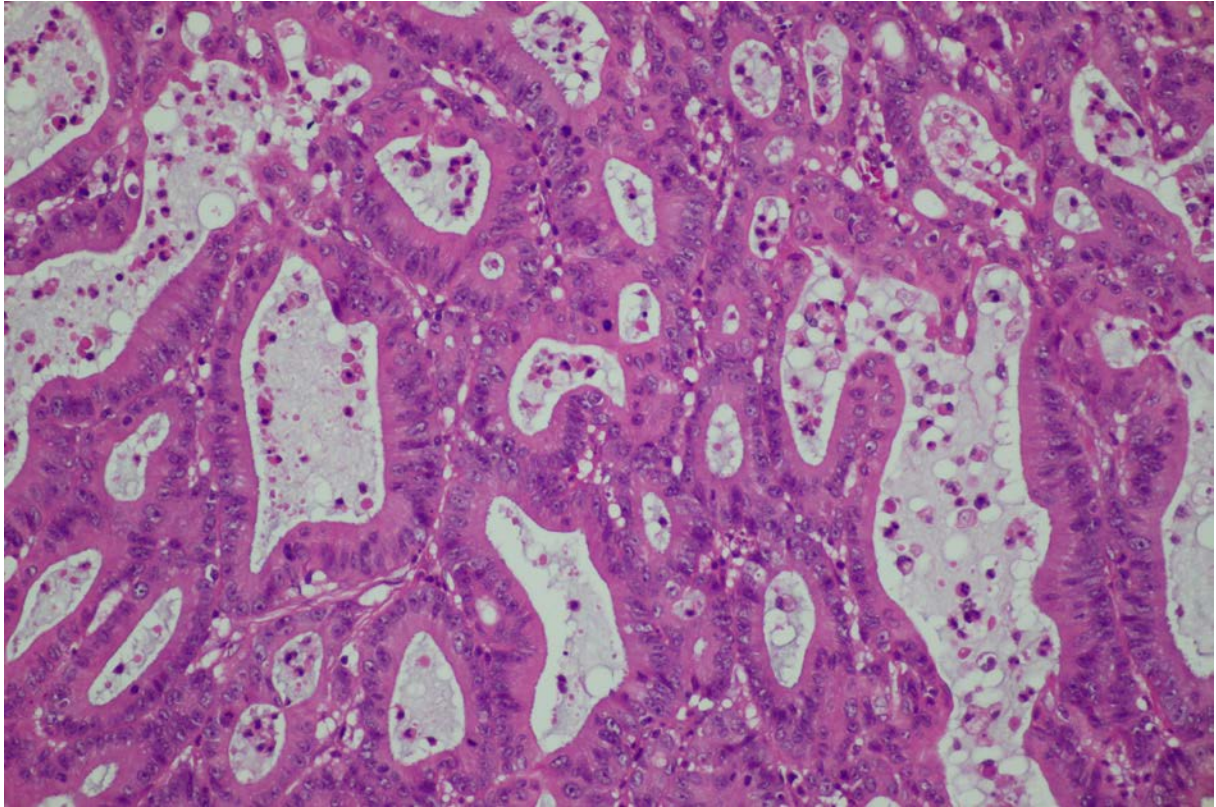
FIGURE 4: Histopathologic sections of the CRCs.

a: Histopathologic section of a WD CRC. (Hematoxylin-eosin stain; original magnification, x200.)
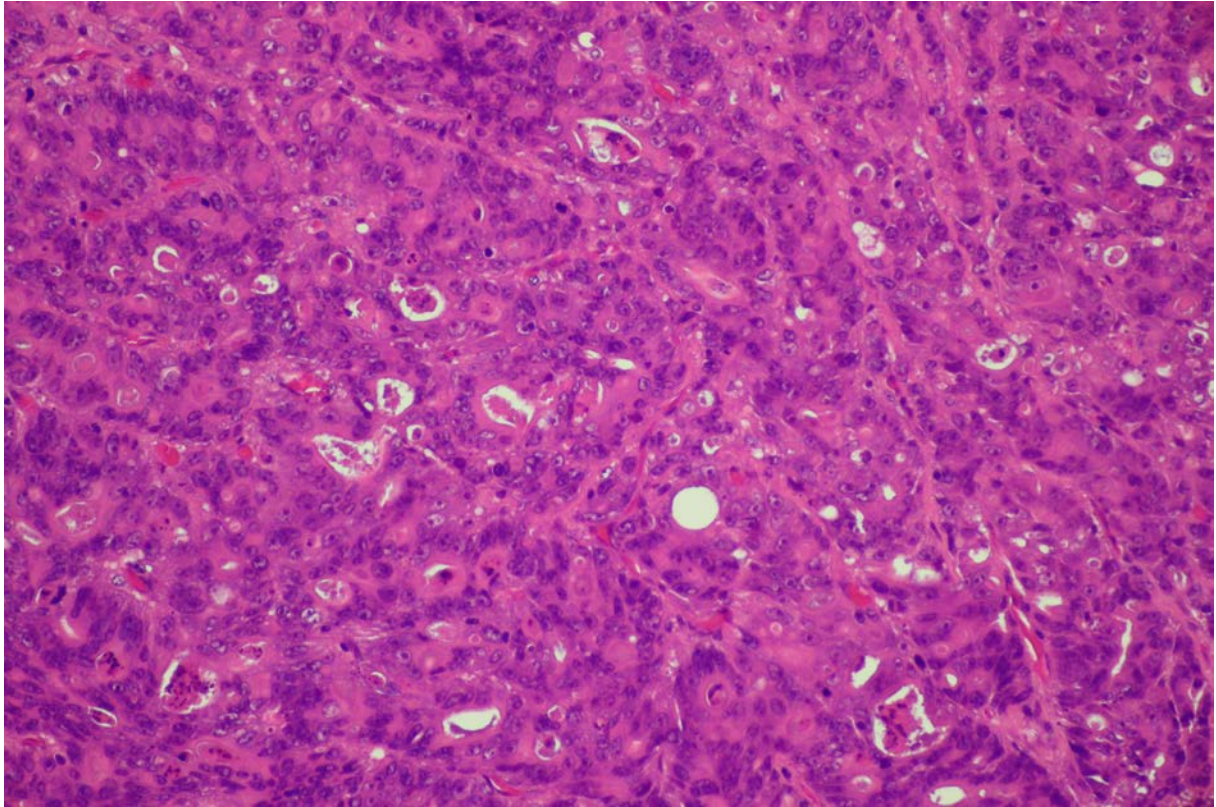
FIGURE 4: Histopathologic sections of the CRCs.

b: Histopathologic section of an MD CRC. (Hematoxylin-eosin stain; original magnification, x200.)
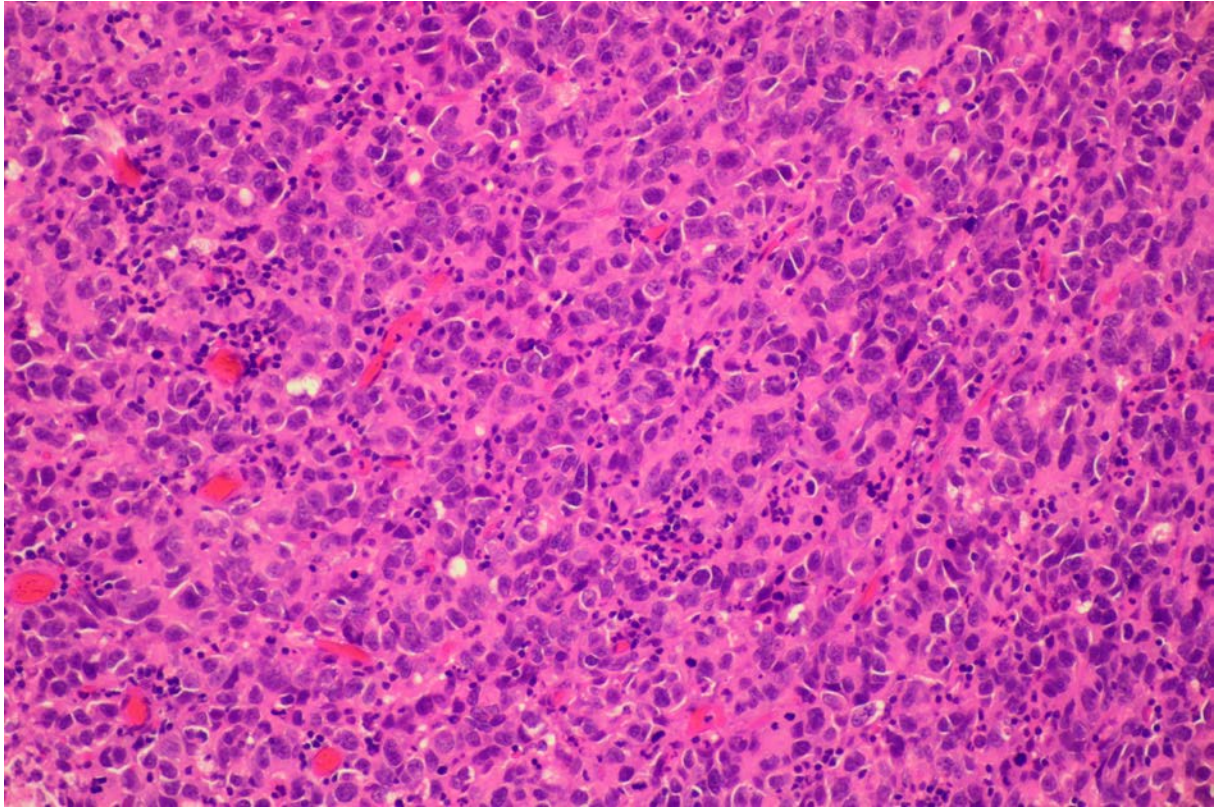
FIGURE 4: Histopathologic sections of the CRCs.

c: Histopathologic section of a PD CRC. (Hematoxylin-eosin stain; original magnification, x200.)
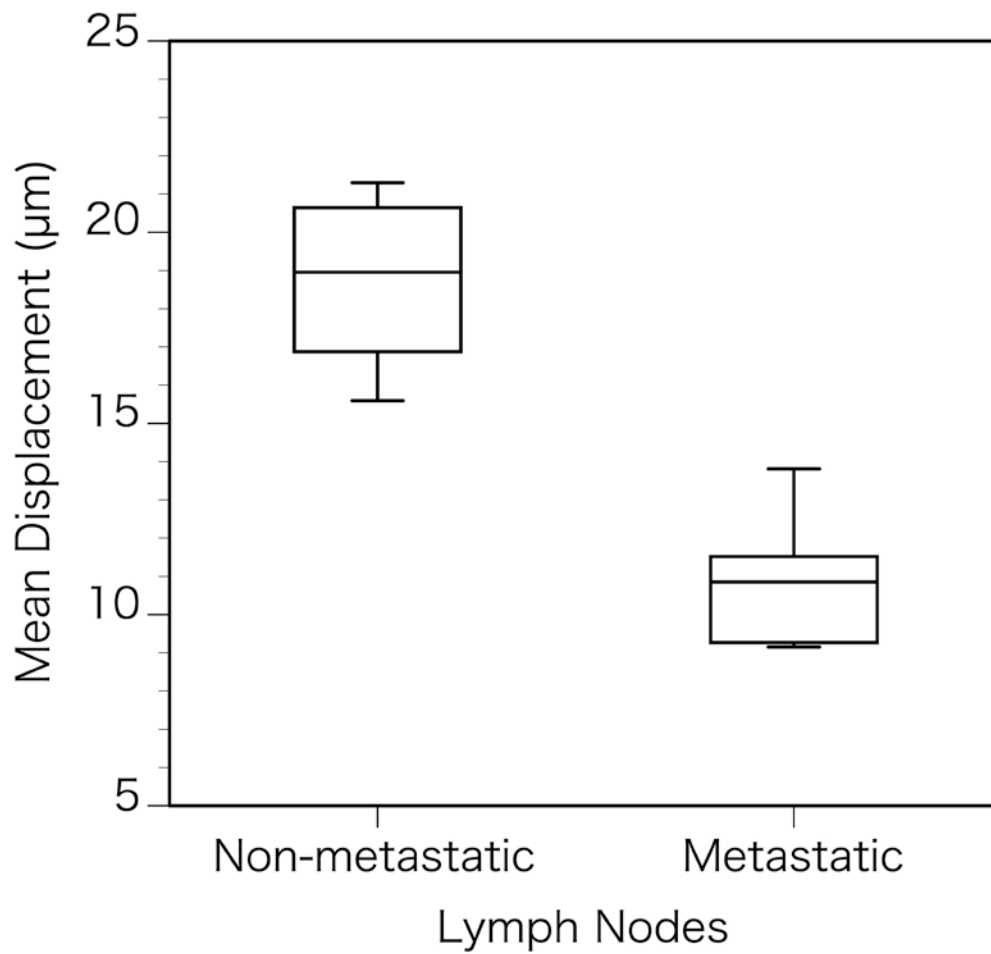
FIGURE 5: Box plots of the QSI parameters in metastatic and non-metastatic LNs in CRC.

a: The MDP values of the metastatic LNs were significantly less than those of the non-metastatic LNs (P < 0.001).
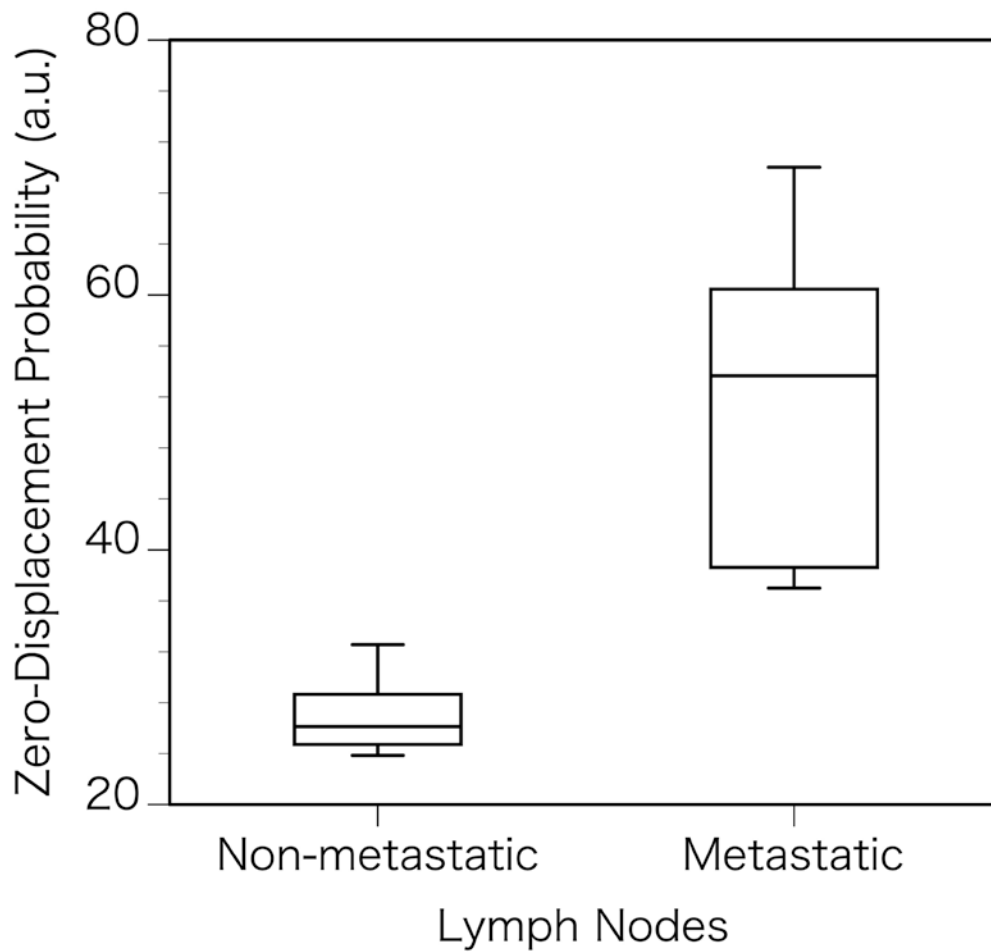
FIGURE 5: Box plots of the QSI parameters in metastatic and non-metastatic LNs in CRC.

b: The ZDP values of the metastatic LNs were significantly greater than those of the non-metastatic LNs (P < 0.001). (a.u. = arbitrary units.)
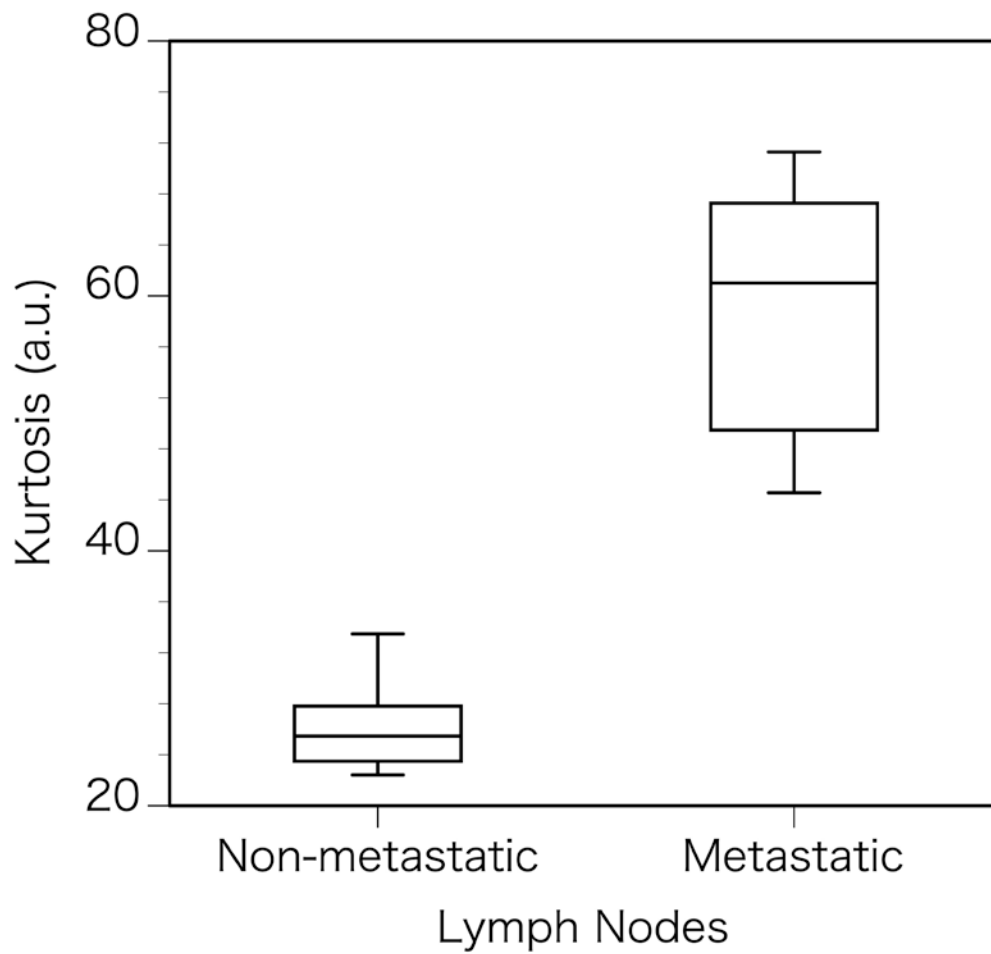
FIGURE 5: Box plots of the QSI parameters in metastatic and non-metastatic LNs in CRC.

c: The K values of the metastatic LNs were also significantly greater than those of the non-metastatic LNs (P < 0.001). (a.u. = arbitrary units.)
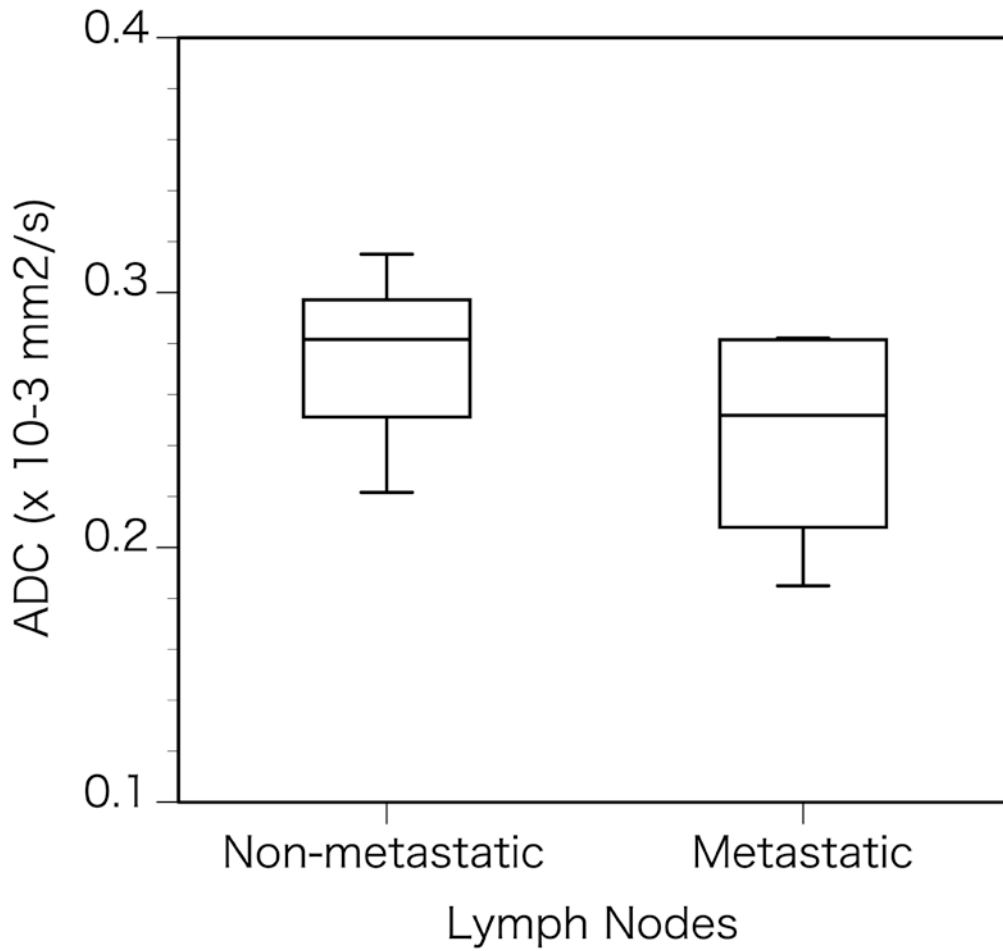
FIGURE 5: Box plots of the QSI parameters in metastatic and non-metastatic LNs in CRC.

d: There were no significant differences between the ADC values of the metastatic and non-metastatic LNs (P = 0.082).
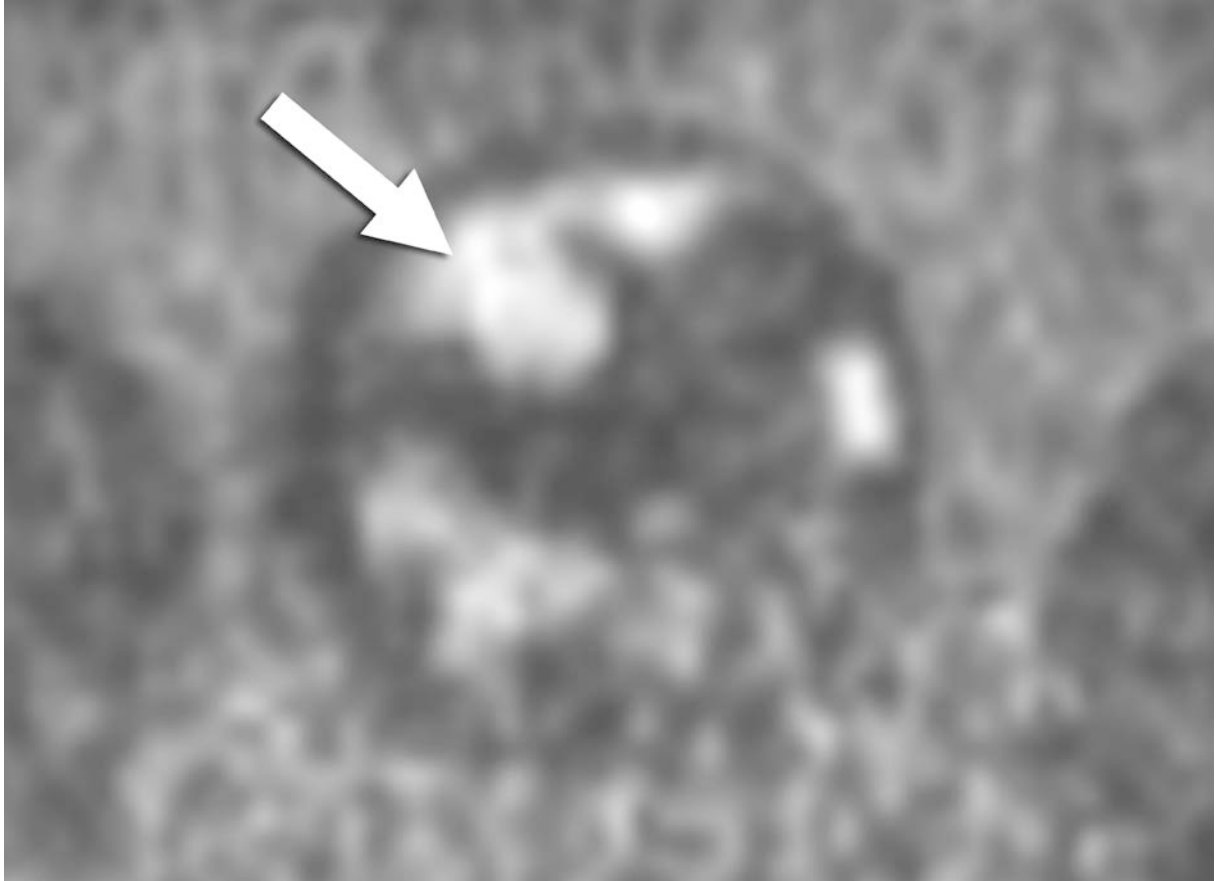
FIGURE 6: Images of a case with metastatic LNs in CRC.

a: DWI (b = 2000 s/mm^2) shows hyperintense, swollen LNs (arrow) in CRC.
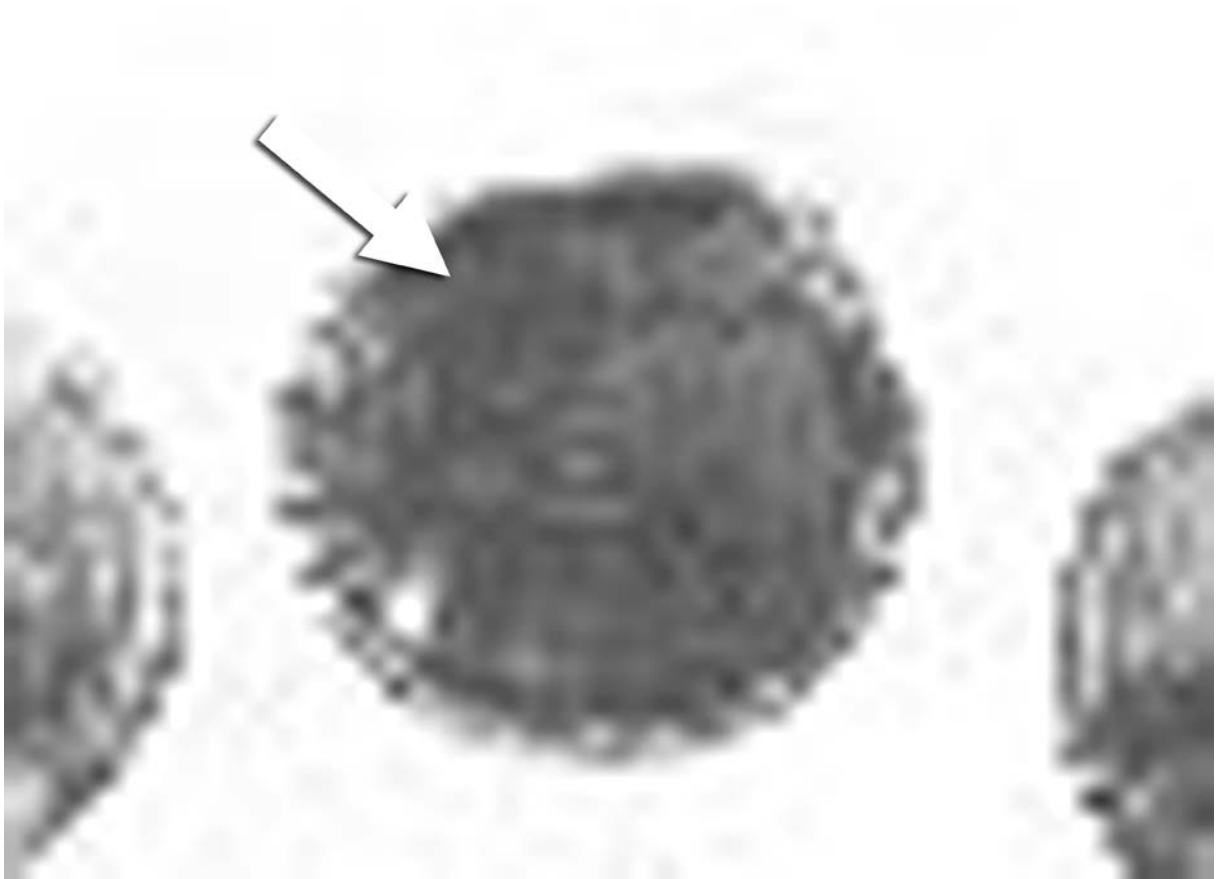
FIGURE 6: Images of a case with metastatic LNs in CRC.

b: MDP map shows the LNs (arrow) are slightly hypointense (MDP = 10.4 μm).
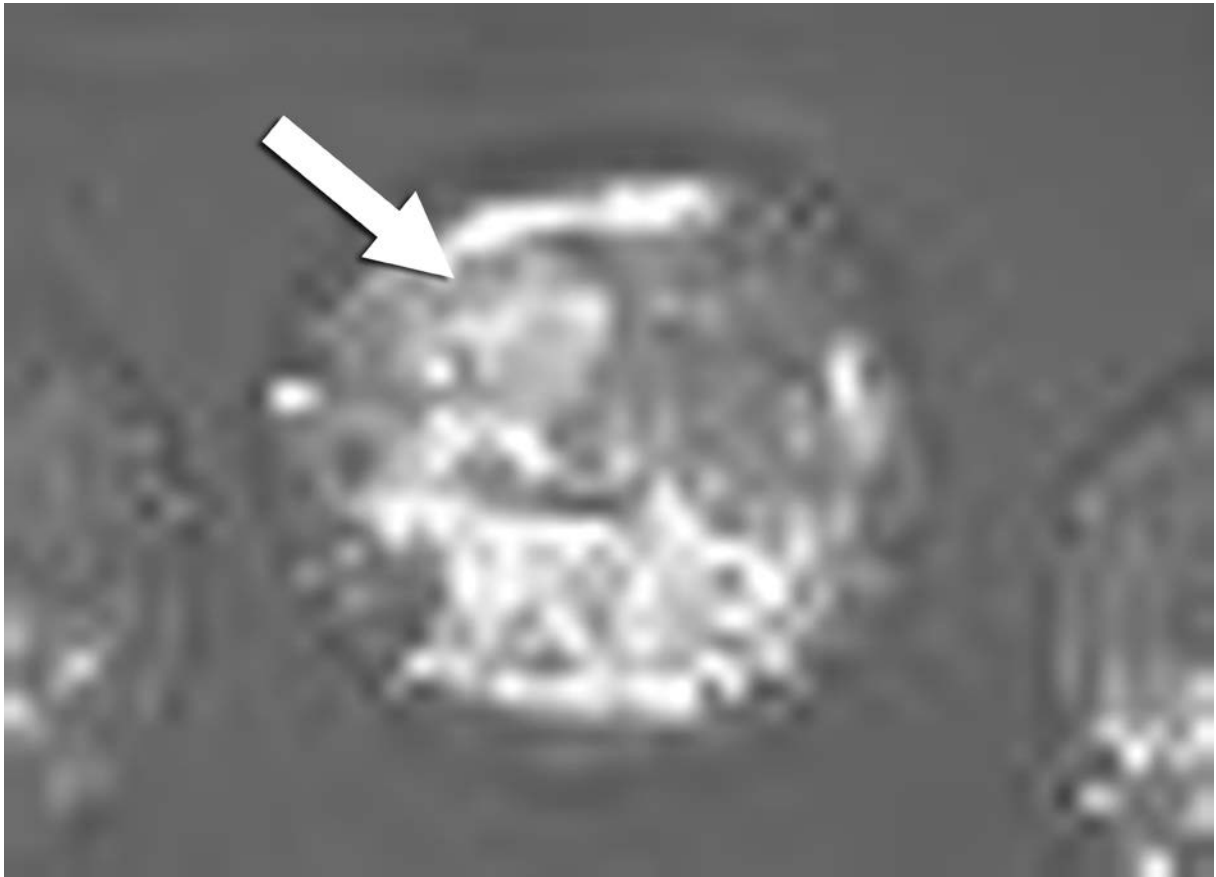
FIGURE 6: Images of a case with metastatic LNs in CRC.

c: ZDP map shows that the LNs (arrow) are slightly hyperintense (ZDP = 52.7 a.u.).
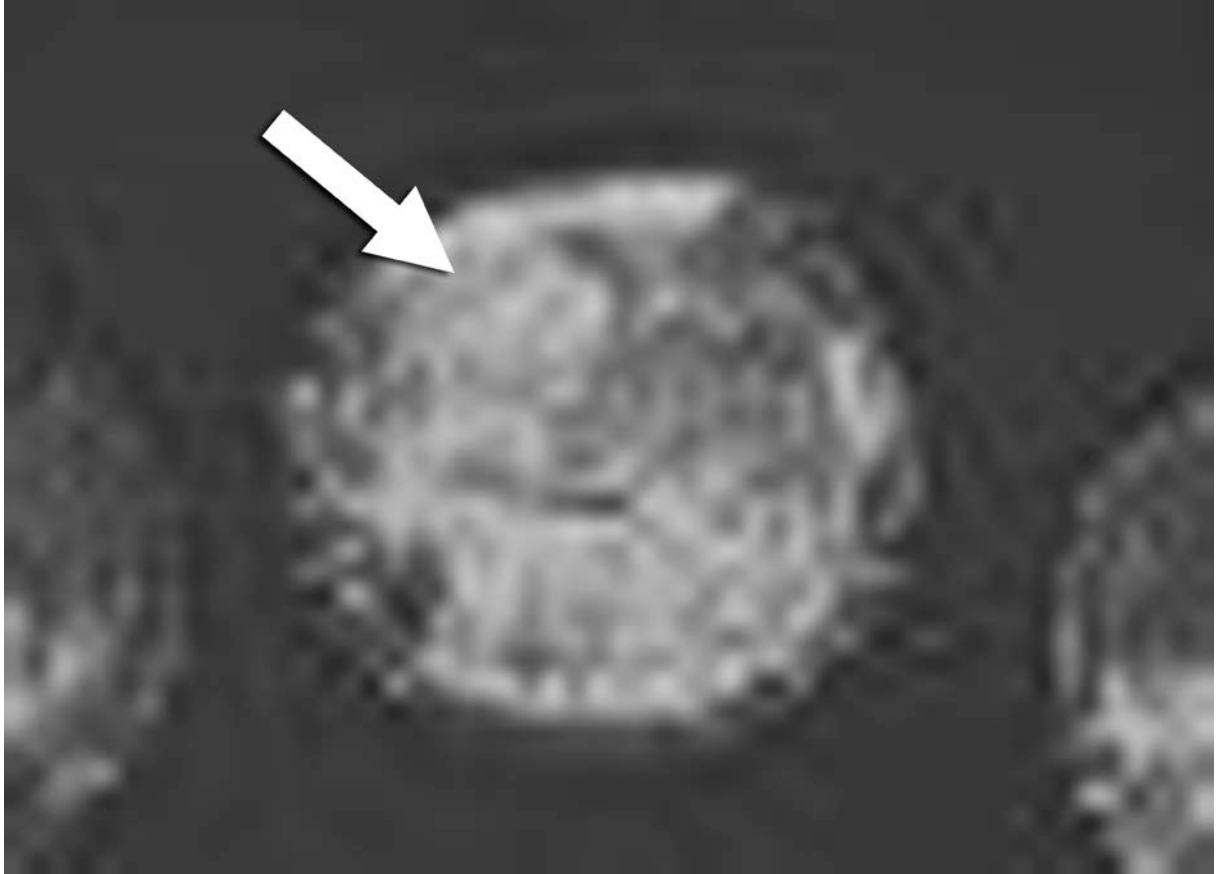
FIGURE 6: Images of a case with metastatic LNs in CRC.

d: K map shows that the LNs (arrow) are slightly hyperintense (K = 60.0 a.u.).
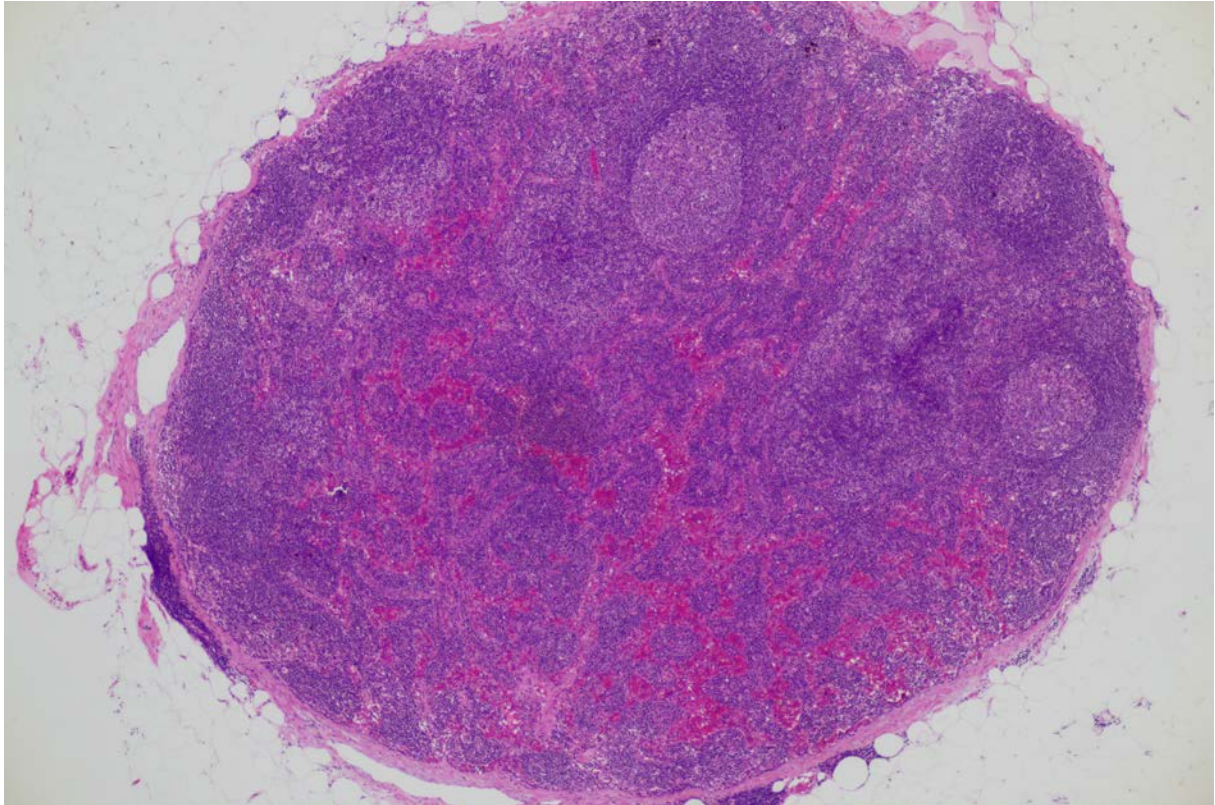
FIGURE 7: Histopathologic sections of non-metastatic and metastatic LNs in CRC.
a: Histopathologic section of a non-metastatic LN. (Hematoxylin-eosin stain; original magnification, x40.)
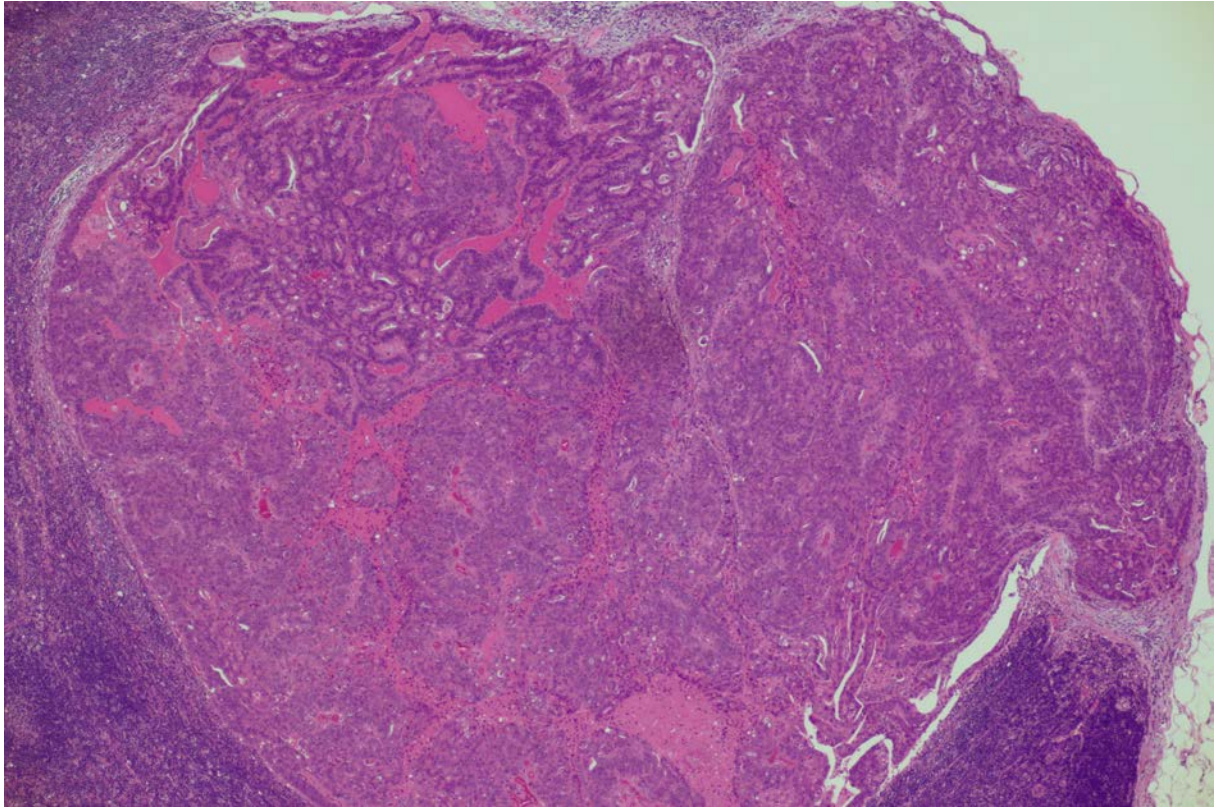
FIGURE 7: Histopathologic sections of non-metastatic and metastatic LNs in CRC.
b: Histopathologic section of a metastatic LN. (Hematoxylin-eosin stain; original magnification, x40.)
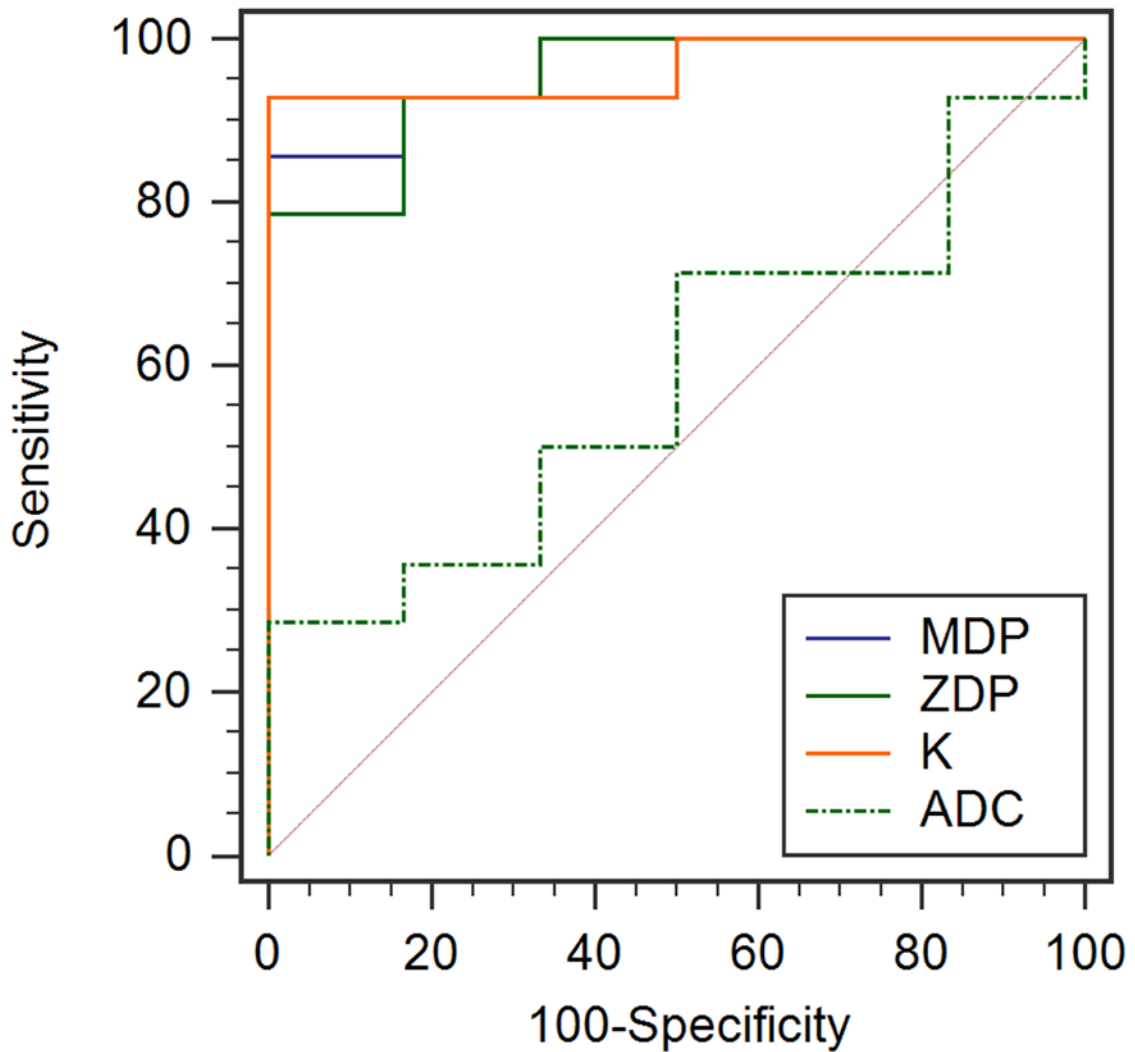
FIGURE 8: ROC curve analyses of the QSI parameters in CRC.

a: ROC curves for differentiating MD or PD from WD CRC. The AUCs for the MDP, ZDP, and K values (0.952, P = 0.0104; 0.952, P = 0.0060; and 0.964, P = 0.0057, respectively) were significantly greater than for the ADC values (0.583). There were no significant differences among the MDP, ZDP, and K values (P = 0.7014−1.0000).
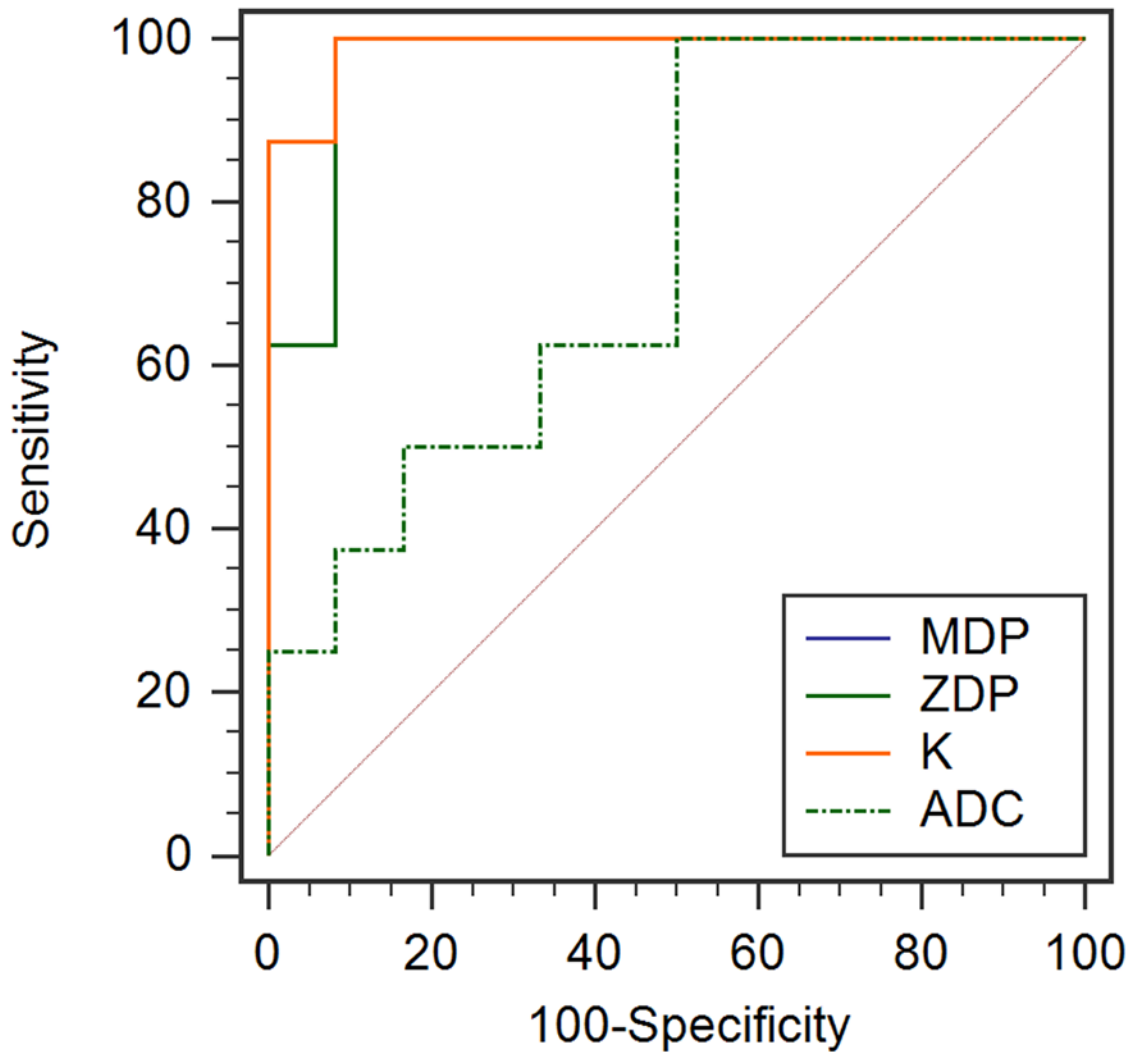
FIGURE 8: ROC curve analyses of the QSI parameters in CRC.

b: ROC curves for differentiating metastatic from non-metastatic LNs in CRC. The AUCs for the MDP, ZDP, and K values (0.990, P = 0.0217; 0.969, P = 0.0192; and 0.990, P = 0.0217, respectively) were significantly greater than for the ADC values (0.740). There were no significant differences among the MDP, ZDP, and K values (P = 0.4028−1.0000).